How the Ancillary Ligand X Drives the Redox Properties of Biscyclopentadienyl Pentavalent Uranium Cp(2)U(N-Ar)X Complexes

Khadidja Talha Yassia, Lotfi Belkhiri, Karine Costuas, Abdou Boucekkine

How the ancillary ligand X drives the redox properties of biscyclopentadienyl pentavalent uranium $Cp_2U(=N\text{-}Ar)X$ complexes.

Khadidja Talha Yassia,[a] Lotfi Belkhiri[a*], Karine Costuas[b] and Abdou Boucekkine[b*]

[a] Laboratoire de Physique Mathématique et Subatomique LPMS, Département de Chimie, Université des Frères Mentouri Constantine 1, 25017 Constantine, Algeria.

[b] Univ Rennes, ISCR UMR 6226 CNRS-Université de Rennes 1, Campus de Beaulieu, F-35042 Rennes Cedex, France.

Abstract:

Relativistic Density Functional Theory (ZORA/DFT) computations coupled with the Conductor-like Screening Model (COSMO) for solvation effects, are used to investigate the redox properties of a series of biscyclopentadienyl pentavalent uranium(V) complexes $Cp_2U(=N\text{-}Ar)X$ (Ar = 2,6-Me_2-C_6H_3 ; X = OTf, C_6F_5, SPh, C=CPh, NPh_2, Ph, Me, OPh, $N(TMS)_2$, $N=CPh_2$). Regarding the U^V/U^{IV} and U^{VI}/U^V couple systems, a linear correlation ($R^2 \sim 0.99$) is obtained ZORA/BP86/TZP level between the calculated ionization energies (IEs) and the measured experimental $E_{1/2}$ half-wave oxidation potentials (U^{VI}/U^V), and between the electron affinities (EAs) and the reduction potentials $E_{1/2}$ (U^V/U^{IV}). The study brings to light the importance of solvation effects that are needed in order to achieve a good agreement between theory and experiment. Introducing spin-orbit coupling corrections slightly improves this agreement. Both the SOMO and the LUMO of the neutral U^V complexes exhibit a majority 5f orbital character. The frontier MOs show a substantial ancillary ligand X σ and/or π character that drives the redox properties. Moreover, our investigations allow estimating the redox potentials of the X=Ph, X=C_6F_5 and $N(TMS)_2$ U^V complexes for which no experimental electrochemical data exist.

Keywords: Uranium(V) complexes, redox half-wave potentials, ZORA/DFT, COSMO, spin-orbit coupling, electron affinity, ionization energy.

Introduction

At the dawn of the 21st century, the redox chemistry of organoactinide complexes has experienced a remarkable revival and growth both experimentally and theoretically.[1-16] Indeed, in addition to the usual ligands such as chloride, carbocyclic ligands (C_5R_5, C_7H_7, C_8H_8) and amides NR_2, the use of a wider range of functionalized groups have led to high oxidation states actinide compounds (> +3) exploiting the stabilization induced by metal–ligand multiple bonds.[17,18] Furthermore, contrarily to the 4f lanthanide electrons which are essentially core electrons, [19] the 5f actinide electrons are involved in the bonding. The nature of the ligands influences the electrochemical, magnetic, and optical propertiesd of actinide systemst.[20,21] Moreover, the investigation of new ligands that could provide thermodynamic stabilization to high-valent uranium species, is interesting first on a fundamental point of view, but also to elaborate new separation techniques and storage methods and for the processing of nuclear wastes from the nuclear plants.[4,8,13,22,23] Indeed, uranium complexes are able to access several oxidation states ranging from U^{II} to U^{VI}.[24,25] Their redox properties and the availability of valence 5f/6d-orbitals to interact make uranium complexes remarkably suitable for exploring new catalytic reactions especially for small molecule activation chemistry.[26-31]

Mixed-ligand metallocene complexes of the type $(C_5Me_5)_2U(X)(Y)$ (X = halogen; Y= triflate, alkyl, phenyl, amide or imide, ketimide, alkoxide/aryloxide, phosphide) have played a crucial role in the development of organometallic actinide chemistry, serving as potent starting materials for the preparation of various functionalized uranium complexes.[7,12,16,32-43] Several research groups were pioneers in the determination of the redox potentials for a wide range of actinide-containing complexes.[3,4,34,35,44-51]

During the last two decades, the Kiplinger's group provided a large number of experimental data (X-ray structures, $E_{1/2}$ half-wave redox potentials, spectroscopic and magnetic measurements) for various U^{IV}/U^{III}, U^{V}/U^{IV} and U^{VI}/U^{V} redox couple of those mixed-ligand complexes.[15,16,34-43] This availability of experimental data is highly valuable, in particular for pentavalent uranium(V) species,[6,7,10,11,18,25,38-40] because of their usual instability leading to their facile disproportionation into uranium(IV) and uranium(VI) species. Even though electron affinity (EA) plays a major role in many areas of pure chemistry, catalysis, materials science and environmental chemistry, its direct measurement is difficult but a wide range of half-wave ($E_{1/2}$) reduction potentials of uranium complexes have been measured.[15,35-51]

However, computational methods are easier-to-implement alternatives which allow determining the redox properties in good agreement with experimental data as shown for example by Rienstra-Kiracofe et *al*.,[52] and more recently by Bateni, et *al.*,[53] and Roy et al.[54] DFT techniques have been used in the case of large actinide-containing molecules gave rise to satisfying accuracy compared to experimental data (within 0.2 eV for redox potentials).[55] Indeed, we showed previously that DFT computed electron affinities for different series of cyclopentadienyl organo-uranium complexes, correlate very well with measured U^{IV}/U^{III} and U^{V}/U^{IV} ($E_{1/2}$) reduction potentials.[11,56-59] This relationship between reduction potentials and electron affinities, was also highlighted by Lobach et *al.*[60] However, despite the great advantages of theoretical investigation toward experimental studies, only few theoretical studies have been devoted to relations between the electronic structure and the redox behavior of actinides complexes. For instance, it is likely that the more pronounced covalent character of the actinide-ligand bonds than lanthanide-ligand ones, involving the 5f electrons will play a role on their electrochemical properties.[4,5,17,18,22]

In view of the rich diversity of organo-uranium complexes, and the importance of the redox chemistry in the reactivity processes,[17,18,27,30,35,61,62] the aim of this work is to investigate the redox properties not only to get access theoretically to the electrochemical potentials but also to corelate these properties to the ligands nature. The target systems are the series of pentavalent bis(cyclopentadienyl) imido-uranium(V) $Cp_2U(=N\text{-}Ar)X$ complexes derived from $[(C_5Me_5)_2U^{V}(=N\text{-}Ar)(X)]$ (Ar = 2,6-$^{i}Pr_2$-C_6H_3 ; X = OTf, SPh, NPh_2, OPh, Me, Ph, C≡CPh, N=CPh_2) complexes (Figure 1), synthetized by Kiplinger's group[38,39] for which U^{V}/U^{IV} and U^{VI}/U^{V} redox ($E_{1/2}$) half-wave potentials have been measured for almost all of them.

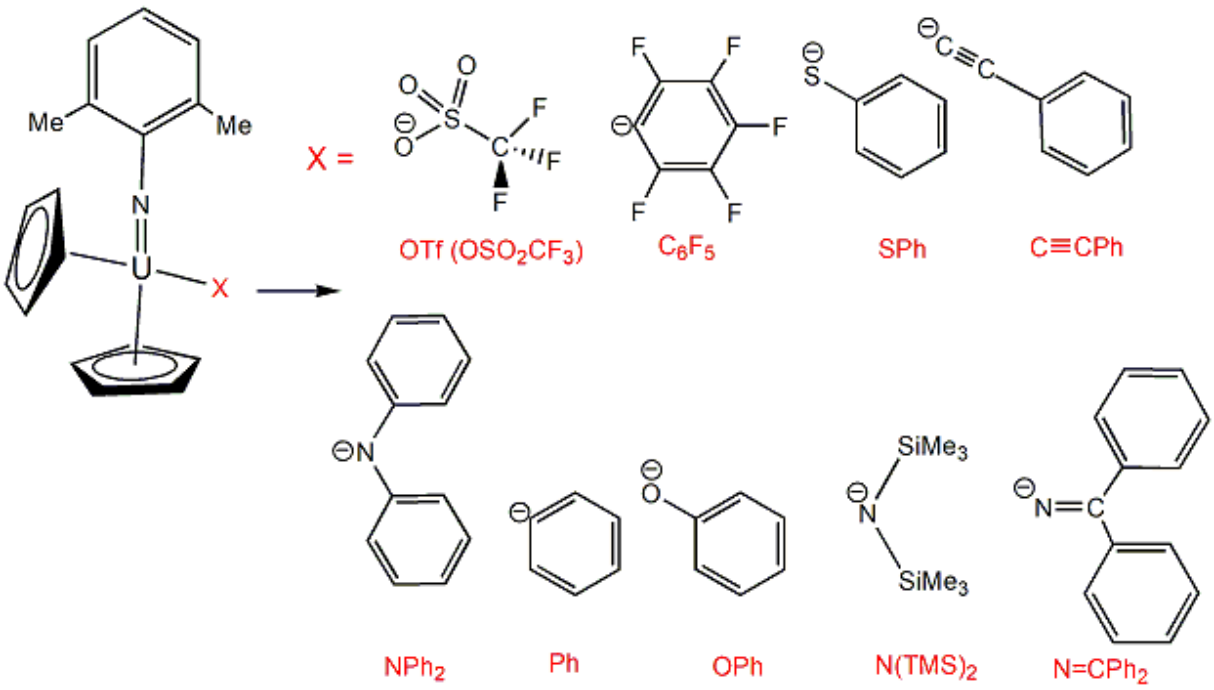

Figure 1: Structures of the $Cp_2U(=N\text{-}Ar)X$ model complexes

As reported by Graves et al.,[39] the spectroscopic analysis of metal-ligand bonding of such complexes shows distinct covalent interactions, which is a clear effect of the σ/π-donation from the ancillary X ligand to the metal U^V center. The electronic influence of the imide NAr group and of the different ancillary X ligands on the redox properties of U(V) complexes is also of high interest especially for disproportionation applications. Moreover, as reported earlier by C. J. Burns and coworkers,[49] electrochemical investigations of uranium(IV) ansa-metallocene $[Me_2Si(C_5Me_4)_2]U(NR)_2$ complexes, containing organoimido functional groups, suggest that the ancillary ligands have the capacity to significantly alter the redox properties of the metal center, and the use of electron donating ancillary ligands seems to stabilize considerably high-valent organo-uranium complexes.

The present study aims first at studying the reliability and accuracy of the used computational technique, *i.e.* relativistic DFT taking into account spin-orbit (SO) coupling, and including solvent effects using the Conductor-like Screening Model (COSMO) approach, and on the other hand at comparing computed EAs and ionization energies (IEs) to electrochemical experimental data. The role of the frontier molecular orbitals (MO) formally involved in most processes, namely the LUMO and SOMO of the neutral U^V complexes during the redox U^V/U^{IV} and U^{VI}/U^V processes will be investigated allowing to highlight the role of the ancillary ligand in the redox properties of these complexes.

Results and discussion

Molecular geometry optimizations

In order to reduce the computational time, the bulky C_5Me_5 groups have been replaced by the unsubstituted C_5H_5/Cp ligand and the Ar = 2,6-$^{i}Pr_2$-C_6H_3 by the 2,6-Me_2-C_6H_3 group in the considered $Cp_2U(=N\text{-}Ar)X$ (X = OTf, SPh, C=CPh, NPh_2, Ph, Me, OPh, N=CPh_2, C_6F_5 and $N(TMS)_2$) complexes (Figure 1). This simplification was successfully used previously,[40,57,58] and will be assessed (*vide infra*). All $Cp_2U(=N\text{-}Ar)X$ geometries were fully optimized at the scalar ZORA/BP86/TZP spin unrestricted level with no symmetry constraints, first in the gas phase and in a second stage in solution (THF solvent) using the COSMO model (see the computational details). In order to check that the optimized geometries are minima on the potential energy surfaces, the vibrational frequencies of the neutral U^V species under consideration were calculated. The molecular structures of the optimized $Cp_2U(=N\text{-}Ar)X$ complexes are depicted in Figure 2. The highest spin states, i.e. doublet ($5f^1$) and triplet state ($5f^2$) for the neutral U^V and anionic (reduced) U^{IV} species respectively, were considered. The optimized structures and atomic coordinates are given in the supporting information (SI).

In Table 1, we report the most relevant computed structural parameters in the gas phase and considering solvation, *i.e*. the U-X bond lengths (where X refers to the first linked ancillary ligand atom to metal), the average U−Cp(centroid) distance, $U{=}N_{Ar}$ imide and $N{-}C_{Ar}$ bond lengths as well as bond angles (°) $U{=}N\text{-}C_{Ar}$ and $Cp_{cent}{-}U{-}Cp_{cent}$, for the three cationic, neutral and anionic U^{VI}, U^V and U^{IV} $Cp_2U(=N\text{-}Ar)X$ complexes. These results are compared to X-ray experimental data when available.

Table 1: Relevant ZORA/BP86/TZP computed distances (Å) and angles (°) of the cationic/neutral/anionic $U^{VI}/U^V/U^{IV}$ $Cp_2U(=N\text{-}Ar)X$ complexes in the gas phase and THF solvated phase (italics) with available X-ray data of the U^V complexes (in bold) and in parentheses a metric deviation (difference between interatomic distances of the X-ray and of the optimized solvated neutral U^V geometries).

	Metal–ligand bond distances (Å)				Angles (°)	
U(VI/V/IV)	U-X	$<U{-}Cp>_{cent}$	$U{=}N_{Ar}$	$N{-}C_{Ar}$	$U{=}N{-}C_{Ar}$	Cp-U-Cp
OTf	2.148/2.258/2.389	2.439/2.458/2.496	1.934/1.961/2.005	1.379/1.383/1.367	175.0/174.9/178.8	123.9/123.9/125.9
	2.147/2.314/2.448	*2.424/2.457/2.495*	*1.943/1.967/2.011*	*1.377/1.384/1.372*	*176.6/172.2/175.3*	*120.8/121.6/122.4*
	2.378 (0.064)	**2.437** (0.020)	**1.957** (0.010)	**1.416** (0.033)	**168.3**	**135.9**
C_6F_5	2.444/2.537/2.640	2.457/2.467/2.514	1.940/1.973/2.018	1.383/1.381/1.369	176.3/173.6/172.9	122.3/121.7/126.5
	2.453/2.545/2.632	*2.435/2.463/2.509*	*1.939/1.974/2.018*	*1.*383/1.381/1.368	*176.1/173.7/172.3*	*121.3/121.6/126.5*

SPh	2.628/2.702/2.793 *2.621/2.718/2.806* **2.723** (0.005)	2.463/2.474/2.514 *2.457/2.470/2.508*	1.946/1.975/2.024 *1.946/1.974/2.021* **1.976** (0.002)	1.382/1.381/1.366 *1.383/1.381/1.366* **1.398** (0.017)	176.3/178.4/177.0 *175.8/177.9/176.3* **171.6**	117.8/123.1/126.5 *116.9/123.1/126.6* **136.2**
C=CPh	2.295/2.392/2.472 *2.302/2.400/2.475*	2.450/2.474/2.525 *2.444/2.469/2.467*	1.942/1.970/2.022 *1.941/1.971/2.024*	1.380/1.381/1.366 *1.381/1.381/1.365*	176.7/177.1/178.9 *177.4/177.2/177.7*	129.4/123.0/125.1 *124.8/122.6/121.9*
NPh_2	2.225/2.300/2.439 *2.223/2.297/2.417* **2.322** (0.025)	2.473/2.494/2.526 *2.464/2.493/2.522* **2.520** (0.027)	1.950/1.977/2.020 *1.952/1.979/2.022* **1.984** (0.005)	1.385/1.382/1.369 *1.384/1.380/1.367* **1.399** (0.019)	174.4/172.7/169.4 *173.8/172.7/170.6* **174.0**	116.6/121.1/120.3 *116.5/120.8/120.5* **125.5**
Ph	2.325/2.396/2.542 *2.320/2.392/2.540*	2.454/2.485/2.529 *2.447/2.488/2.524*	1.954/1.981/2.030 *1.954/1.984/2.032*	1.384/1.381/1.367 *1.385/1.380/1.365*	174.1/172.8/172.3 *174.6/172.9/171.5*	123.1/123.5/123.6 *122.6/124.3/124.4*
Me	2.343/2.421/2.495 *2.345/2.421/2.497*	2.453/2.486/2.534 *2.454/2.485/2.526*	1.943/1.979/2.033 *1.945/1.979/2.034*	1.380/1.380/1.363 *1.379/1.380/1.362*	173.7/173.5/174.7 *172.7/173.5/173.8*	121.1/124.6/124.1 *122.5/124.5/123.9*
OPh	2.077/2.124/2.206 *2.078/2.124/2.199*	2.456/2.483/2.542 *2.448/2.481/2.534*	1.955/1.984/2.032 *1.955/1.986/2.034*	1.378/1.379/1.365 *1.379/1.378/1.363*	177.2/176.1/177.6 *176.3/176.1/177.0*	124.2/124.1/121.1 *124.3/123.7/120.7*
$N(TMS)_2$	2.174/2.280/2.419 *2.174/2.275/2.389*	2.491/2.515/2.551 *2.481/2.504/2.550*	1.955/1.976/2.025 *1.956/1.979/2.029*	1.381/1.379/1.366 *1.381/1.377/1.362*	172.5/171.6/168.0 *172.2/171.7/168.5*	115.1/116.1/117.1 *115.0/116.1/117.1*
$N=CPh_2$	2.111//2.158/2.178 *2.109/2.164/2.174* **2.199** (0.035)	2.465/2.510/2.537 *2.457/2.496/2.536* **2.488** (0.009)	1.958/1.993/2.035 *1.958/1.996/2.037* **2.012** (0.028)	1.380/1.379/1.366 *1.380/1.378/1.364* **1.391** (0.013)	176.7/175.9/176.9 *173.9/176.0/176.8* **174.6**	132.2/132.4/128.4 *131.9/132.0/128.4* **138.3**

The calculated geometrical parameters of $Cp_2U(=N\text{-}Ar)X$ model systems, are in good overall agreement with the available experimental X-ray data, especially when taking into account the solvent effect. The largest deviation of *ca*. 0.06 Å is found for the metal-ligand U–X and $U=N_{Ar}$ bond lengths (Table 1) explained by the absence of the steric hindrance of the bulky pentamethylcyclopentadienyl (C_5Me_5) ligand in our model complexes.[38,39] This good agreement gives confidence in the reliability of the ZORA/BP86/TZP method in computing molecular 5f-complexes geometries. Notably, the lengthening of the metal-ligand U–X and $U=N_{Ar}$ bond distances when going from the neutral U^{V} to anionic (reduced) U^{IV} species is in line with uranium ionic radii variation.[63]

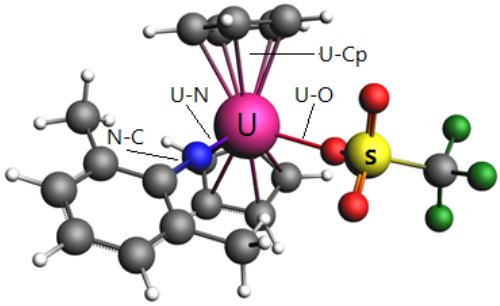

$Cp_2U(=N\text{-}Ar)(OTf)$

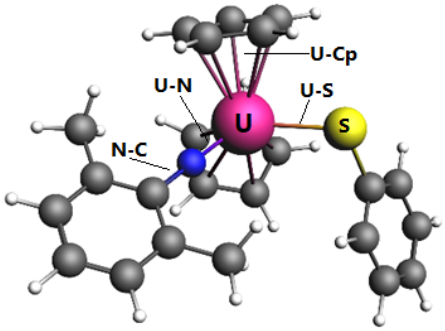

$Cp_2U(=N\text{-}Ar)(SPh)$

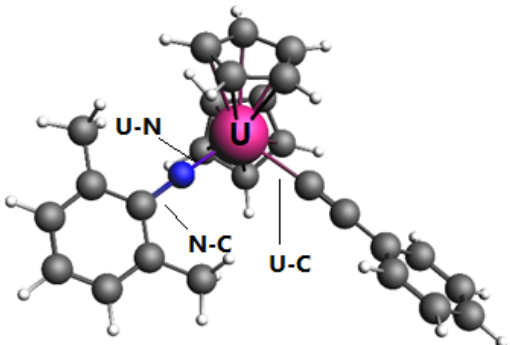

$Cp_2U(=N\text{-}Ar)(C{\equiv}CPh)$

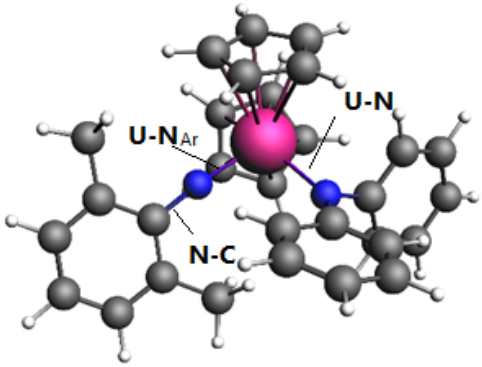

$Cp_2U(=N\text{-}Ar)(NPh_2)$

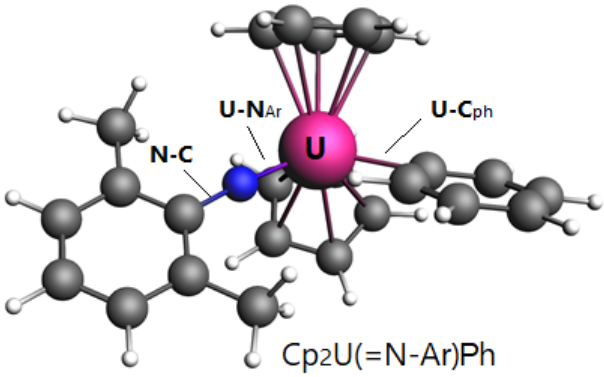

$Cp_2U(=N\text{-}Ar)Ph$

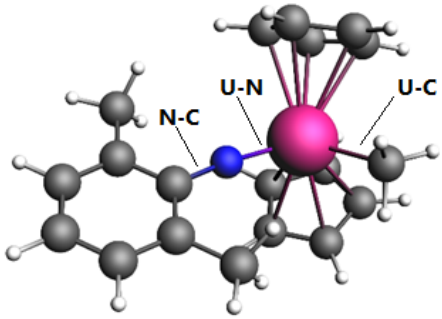

$Cp_2U(=N\text{-}Ar)Me$

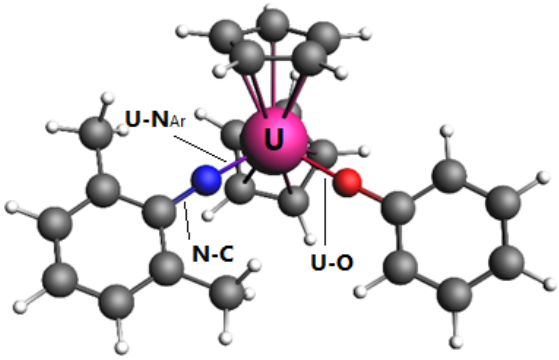

$Cp_2U(=N\text{-}Ar)(OPh)$

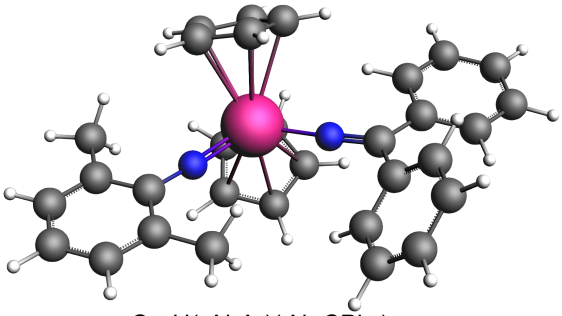

$Cp_2U(=N\text{-}Ar)(\text{-}N{=}CPh_2)$

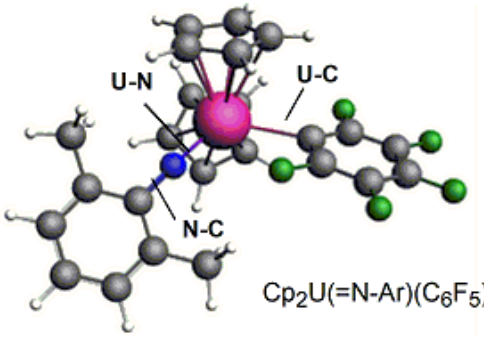

$Cp_2U(=N\text{-}Ar)(C_6F_5)$

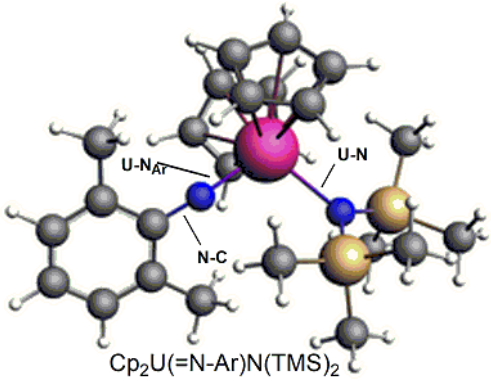

$Cp_2U(=N\text{-}Ar)N(TMS)_2$

Figure 2: ZORA/BP86/TZP optimized molecular structures in the gas phase of the $Cp_2U(=N\text{-}Ar)X$ (X = OTf, SPh, C=CPh, NPh_2, Ph, Me, OPh, $N=CPh_2$,C_6F_5, $N(TMS)_2$) complexes.

The oxidation process from U^V neutral to U^{VI} cationic species induces a shortening of the metal–ligands bond lengths (*ca*. 0.08 Å). Oxidation affects clearly the metal–ligand U–X and $U=N_{Ar}$ bond distances. The $N–C_{Ar}$ bond lengths are not significantly altered upon oxidation (by *ca*. 0.002 Å) contrarily to the reduction process that induces shortening of *ca.* 0.02 Å. This is presumably due to the lack of metal-to-ligand back-donating effect within the imide $U=N–C_{Ar}$ coordination for the oxidized U^{VI} ($5f^0$) cationic species. Indeed, keeping in mind that the U(V) LUMO and SOMO are pure metallic 5f MO during the reduction process, the U=N imide bond length gets longer when passing from the neutral U(V) to the anionic U(IV) species as a result of the uranium ionic radii variation,[62] accompanied by the $N–C_{Ar}$ shortening, as shown in Table **1**. This latter result is likely to follow from the weak back-donating effect consecutive to the metal-ligand U=N bond lengthening. This latter is expected as the SOMO of the neutral U(V) $5f^1$ species moving to the U(VI) $5f^0$ are pure metallic FMO, while the U(V) SOMO-1 is a π U(5f)-N(2p) MO as shown in Figure 7. The oxidized U(VI) species, exhibiting a SOMO U(VI) $5f^0$, which traduces the ligand-to-metal bonding π U(5f)-N(2p) MO as shown on Figure 7, would not favor any back-donation into the ligand orbitals which explain the quasi-constant $N–C_{Ar}$ bond distances. Furthermore, the oxidized U(VI) species, exhibiting a $5f^0$ FMO, therefore, would not favor any metal-ligand back-donation into the ligand orbitals which explain the quasi-constant $N–C_{Ar}$ bond distances.

The Cp–U–Cp angle and $U=N–C_{Ar}$ are slightly affected (by *ca*. 3° and *ca*. 1° respectively). Furthermore, although X-ray data are not available for several complexes, the $U=N_{Ar}$ metal-imide bond distances computed taking into account the solvent effect, *i.e.*, 1.974 Å, 1.979 Å and 1.986 Å for X = C_6F_5, Me and OPh species respectively, compare well with observed uranium(V)-imide multiple bond lengths ranging from **1.957** to **2.012** Å.[37,38] Notably, the computed $U^V–C_{Ph}$ (2.392 Å), $U^V–C_{Me}$ (2.421 Å) and $U^V–O$ (2.124 Å) distances for the Ph, Me and OPh complexes, respectively, are in good agreement with the crystal structure data obtained for $U^V–CN$ (**2.491**(7) Å X-ray *vs.* DFT 2.488 Å) and $U^V–O$ (**2.102(4)** Å X-ray *vs.* DFT 2.111 Å) of the $[Et_4N][U^VO(CN)[N(SiMe_3)_2]_3]$ uranium(V) cyanide and $U^V(ONap)_2[N(SiMe_3)_2]_3$ (Nap = Naphthyl) complexes.[64]

For the $N(TMS)_2$ complex considered in solution, the computed metal–amide $U^V–N$ (2.275 Å) bond lengths can be compared to analogous interatomic distances in the $(C_5Me_5)_2U^V(=N\text{-}Ar)(NPh_2)$[40] complex ($U^V–N$ = **2.322** Å X-ray *vs*. DFT 2.297 Å). The C_6F_5 complex exhibits a

computed U^{V}–C distance equal to 2.545 Å whereas in the Ph species the U^{V}–C_{Ph} bond length is 2.392 Å. Moreover, the computed metal–imide U^{V}=NAr bond distances, *i.e.*, 1.974 and 1.979 Å for the C_6F_5 and $N(TMS)_2$ complexes, compare well with similar bond lengths in the literature. The U^{VI}–C_{Ph} = 2.320 Å and U^{VI}–C_{Me} = 2.345 Å bond distances of the computed uranium(VI) (X= Ph, Me) can also be compared formally to the scarce uranium(VI)−methyl and −acetylide X-ray structures, $U^{VI}OR[N(SiMe_3)_2]_3$ complexes with R = −C≡CPh, $-CH_3$ which exhibit **2.337**(14) and **2.343**(4) Å short U–C bond lengths, respectively.[65]

Interestingly, the computed shorter U=N_{Ar} bond lengths as well as the nearly lined up U=N–C_{Ar} atoms, are reminiscent of multiple uranium–imido bond, well in line with the corresponding geometrical parameters observed for the structurally characterized high-valent (U^{IV}, U^{V}, U^{VI}) imido species.[7,27,35-41,49,59] As expected, the computed Cp(centroid)–U–Cp(centroid) angles in the U^{V}/U^{IV} redox couple are also well reproduced, with typical values of *ca*. 125°, agreeing with the familiar pseudo tetrahedral bent sandwich configuration of the Cp_2U molecular fragment. It is noteworthy that the geometry of the Cp_2U(=N-Ar) moiety is influenced by the nature of the X ancillary ligand. For instance, the U–Cp_{cent} and U=N_{Ar} distances are varying from 2.447 to 2.496 Å and 1.954 to 1.996 Å, respectively for the compounds under consideration in agreement with X-ray data.

The strength of the electron donating character of the ancillary X ligand (OTf, C_6F_5, SPh, C=CPh, NPh_2, Ph, Me, OPh, $N(TMS)_2$, N=CPh_2), seems to affect the U=N_{Ar} bond distances. Indeed, the very weak σ-donation of the triflate OTf ligand leads to the shortest U^{V}=N_{Ar} bond distances (1.967 Å) computed in solution, agreeing perfectly with the shortest X-ray observed (**1.957** Å) one. In opposite, the most polarizable N=CPh_2 ligand that is a better σ/π-donor than the other ancillary X ligands, leads to the longest U^{V}=N_{Ar} bond distances (1.996 Å computed *vs*. X-ray **2.012** Å). This evolution of the U=N_{Ar} bond distances correlates well with the increasing donating ability of the X ligand that is OTf < SPh < C=CPh < OPh ~ Me ~ Ph < NPh_2 < N=CPh_2, as given by Kiplinger and coworkers following the NMR analysis of the actual $(C_5Me_5)_2U$(=N-Ar)X complexes.[39]

As reported,[39,40] the observed variability of the half-wave reduction potentials ($E_{1/2}$) across this series of complexes reflects the driving role of the ancillary ligand X. Therefore, the OTf U^{V} complex that exhibits the lowest reduction potential (**-1.21** V) is the easiest to reduce; the poor electron donating OTf ligand is accompanied by a stronger coordination from the imide (=N-Ar) group towards the metal as the U^{V}=N computed bond length is the shortest (1.967 Å) agreeing well with the observed one (X-ray **1.957** Å). In opposite, the ketimide N=CPh_2

ligand appearing as the strongest donor and exhibiting the highest negative reduction potential (**-1.84** V) is accompanied with the longest U^{V}=N bond length (computed 1.996 Å *vs*. X-ray **2.012 Å**). A slight shortening of the N−C_{Ar} bond lengths when passing from the U^{V} to the U^{IV} species. The reduction process affects the metal–imide U=N_{Ar} bond length whose lengthening is likely to reduce metal-to-imide back-donation. For the ketimide N=CPh_2 complex the metal-imide U^{V}=N_{Ar} bond lengthens from 1.996 to 2.037 Å *vs*. the N−C_{Ar} shortening from 1.378 to 1.364 Å for U^{V} *vs*. U^{IV} couple, respectively (Table 1). Therefore, a subtle relationship exists between purely electrostatic effects (*e.g.*, with OTf) and more intrinsic σ- and π-bonding interactions (*e.g.*, ketimide N=CPh_2) that drives the electron density transfer to the metal center and therefore impacts not only the redox energetics but also the metal-ligand U–X and U=N_{Ar} bond distances.

Electronic structure analyses.

The analyses in this section are all performed using the computed results using the optimized equilibrium geometries obtained at the ZORA/BP86/TZP level and taking into account solvation effects (THF). The Mulliken population Analysis (MPA)[66] has been carried out to bring some light on the evolution of the metal spin density (ρ) and of the 5f orbitals spin populations upon the redox processes. Despite its known drawbacks, MPA allows a qualitative description of charge transfers and bonding interactions in molecular systems. The Natural Population Analysis (NPA)[67] was also performed to probe the covalence in f-element complexes.[68] Hirshfeld's analyses which provide metal net charges (q) and thus major electron transfers occurring in our systems are also considered.[69] The computed data, namely MPA uranium spin densities (ρ) computed as the difference between the α and β metal spin populations and the 5f orbitals spin populations (difference between the α and β orbital spin populations) as well as Hirshfeld net charges are reported in Table 2.

Table 2: ZORA/BP86/TZP MPA metal spin densities (ρ), 5f spin populations and Hirshfeld metal net charges (q) for the $U^{VI}/U^{V}/U^{IV}$ $Cp_2U(=N\text{-}Ar)X$ species, in THF solvent.

Structures Cp/Cp*	MPA				Hirshfeld		
	Metal spin density		5f spin population		q metallic net charge		
	$\rho(U^{V})$	$\rho(U^{IV})$	$5f^1$ (U^{V})	$5f^2$ (U^{IV})	U^{VI}	U^{V}	U^{IV}
OTf	1.22	2.18/2.21	1.11	2.01	+0.75	+0.68	+0.58
C_6F_5	1.23	2.17	1.13	1.99	+0.70	+0.64	+0.54
SPh	1.24	2.20	1.13	2.00	+0.63	+0.60	+0.50
C=CPh	1.20	2.14	1.08	1.96	+0.72	+0.64	+0.54
NPh_2	1.25	2.15	1.13	1.92	+0.66	+0.62	+0.54
Ph	1.24	2.15	1.14	1.97	+0.69	+0.62	+0.54
Me	1.22	2.15	1.13	1.96	+0.75	+0.66	+0.54
OPh	1.22	2.19	1.10	1.88	+0.75	+0.66	+0.55
$N(TMS)_2$	1.23	2.21	1.09	1.91	+0.68	+0.63	+0.55
$N=CPh_2$	0.97	1.80	0.90	1.63	+0.70	+0.64	+0.56

The formally occupation of the 5f metal orbitals are expected to be $5f^1/5f^2$ in U^{V}/U^{IV} complexes. In the studied systems the uranium spin densities (Table 2), are higher than 1 and 2 respectively for the neutral and anion U^{V}/U^{IV} complexes, except in the case of the $N=CPh_2$ complexes (0.97 and 1.80). The computed 5f spin population in the neutral U^{V} complexes is slightly higher than the $5f^1$ occupation of the uranium centre, indicating that a negative spin density is spread over the ligands. It is worth to note that the lowest spin populations (0.90/1.63) are obtained for the U^{V}/U^{IV} ketimide $N=CPh_2$ species. This is in line with the back-donation ability of the ketimide ligand reinforcing the covalent character of the metal-ligand bonding interactions (*vide infra*).

The Hirshfeld's analysis that gives access to the metallic net charges evolution from the cation U^{VI} to the neutral U^{V} then to the anion U^{IV} species, shows that the computed values are largely lower than the formal ion charge +6, +5 and +4, respectively, indication strong ligand-to-metal donation that contributes to the stabilisation of the high oxidation states (>+3) of the uranium species. The MPA and NPA analyses (detailed in SI; Table S1) lead to the same trend regarding the metallic charges. Considering Hirshfeld's analysis, it can be seen that the uranium charges increase slightly with the oxidation state of the central metal as previously noticed,[59] in line with chemical intuition.[70] Indeed, this can be exemplified by the ketimide $N=CPh_2$ case, where the uranium net charge increases from +0.56 for the anion U^{IV}

species to +0.64 for neutral U^{V} then to +0.70 for cation U^{VI} one. Moreover, the ligand-to-metal donation increases with the uranium oxidation state; this effect should induce the decrease of the global net charges of the ligands. In Table 3, the computed Hirshfeld global charges of the UCp_2 + NAr + X moieties of the different complexes are collected, using the fragments analysis implemented in the ADF suite of programs (see computational details). The numbers −1, 0 and +1 indicate respectively the anionic U^{IV}, the neutral U^{V}, and the cationic U^{VI} species. For example, considering the anionic U^{IV} species, the $(Cp_2U)^{2+}$, $(NAr)^{2-}$ and X^{-} model fragments are computed. The global net charges of the different UCp_2, NAr and X moieties allow revealing the amount of charge transfer upon interaction of those fragments upon the U^{V}/U^{IV} reduction and U^{VI}/U^{V} oxidation processes. The charge transfer from the ligands to the metal is highlighted by the weak negative charges carried by the NAr and X donor ligands, becoming weaker with the highest uranium oxidation states.

Table 3: ZORA/BP86/TZP Hirshfeld global net charges of the [Cp_2U + NAr + X] fragments for the cation (U^{VI}), neutral (U^{V}) and anion (U^{IV}) complexes, in THF solvent.

Complex charge	−1			0			+1		
fragments	$(Cp_2U)^{2+}$	$(NAr)^{2-}$	X^{-}	$(Cp_2U)^{3+}$	$(NAr)^{2-}$	X^{-}	$(Cp_2U)^{4+}$	$(NAr)^{2-}$	X^{-}
OTf	+1.05	−1.19	−0.86	+1.70	−0.92	−0.77	+2.27	−0.68	−0.59
C_6F_5	+1.06	−1.20	−0.86	+1.70	−0.94	−0.75	+2.33	−0.73	−0.60
SPh	+1.03	−1.21	−0.82	+1.64	−0.97	−0.67	+2.22	−0.81	−0.41
C=CPh	+1.05	−1.21	−0.84	+1.65	−0.95	−0.70	+2.28	−0.76	−0.52
NPh_2	+0.98	−1.25	−0.73	+1.56	−1.04	−0.52	+2.14	−0.86	−0.28
Ph	+1.06	−1.25	−0.81	+1.64	−1.01	−0.62	+2.30	−0.83	−0.47
Me	+1.05	−1.24	−0.81	+1.68	−0.95	−0.73	+2.37	−0.77	−0.60
OPh	+1.12	−1.22	−0.90	+1.63	−1.01	−0.62	+2.20	−0.78	−0.42
$N(TMS)_2$	+1.04	−1.28	−0.76	+1.62	−1.03	−0.59	+2.23	−0.85	−0.38
$N=CPh_2$	+0.94	−1.26	−0.68	+1.55	−0.99	−0.56	+2.15	−0.88	−0.26

Taking the ketimide $N=CPh_2$ uranium complex as a study case, it can be seen that the global negative net charge carried by the imide NAr donor group, decreases significantly: it is equal to −1.26 for the anionic (U^{IV}) species, −0.99 for the neutral U^{V} molecule, and becomes −0.88 in the cationic U^{VI} one. Interestingly, the net charge carried by the ancillary X ketimide ligand decreases from −0.68 (U^{IV}), to −0.56 (U^{V}) and reaches only −0.26 in the cationic U^{VI} species.

Regarding the global negative net charges carried by the imide NAr and ancillary donor groups, the $N(TMS)_2$ complex exhibits the same trends as the ketimide $N{=}CPh_2$ species.

In the case of poor electron donor ancillary ligands *e.g.*, the triflate system, the OTf net charge decreases from −0.86 (U^{IV}), to −0.77 (U^{V}) and finally reaches −0.59 (U^{VI}). Similarly, for the electron withdrawing fluorinated C_6F_5 group, the global negative charge carried by this latter ligand in the complex, is high for the three-oxidation states U^{VI}, U^{V} and U^{IV} as noted for the triflate system compared to the other species, sustaining their weak donating ability.

These results correlate well with the ligand-to-metal donation increasing with the uranium oxidation state (Table 2), confirming also that the ancillary ketimide $N{=}CPh_2$ ligand exhibiting the lowest global negative charges during the redox process is the strongest electron donating ligand. It appears that its strong donation ability compensates the relative low electron donation from the NAr imide ligand. The electron-donation interplay revealed by the Hirshfeld's charge transfer analysis (Table 3) for the ketimide ancillary ligand comparatively to the other groups, correlates well with the experimental trends.[39] Indeed, the relative lowest negative charges (*e.g.* –0.56 for U^{V} species) borne by the ketimide ligand, confirms its stronger electron donation towards the central metal making the corresponding complex the most difficult to reduce as sustained by the most negative half-wave potential ($E_{1/2}$ = **–1.84** V) in the series of complexes. In opposite, the triflate ancillary group bearing the highest negative charge (*e.g.* –0.77 for the U^{V} complex) in agreement with its electron−poor donation ability, renders the complex the most easily reducible with the less negative half-wave potential ($E_{1/2}$ = **–1.21** V).[39] This is also the case for the fluorinated C_6F_5 group which exhibits a weak charge transfer leading to a high negative global charge (*i.e.* –0.75 for U^{V} species). As reported by Kiplinger and coworkers,[38] combining absorption spectroscopic data, the ketimide and triflate groups are classified as the stronger *vs*. weaker electron-donor ancillary ligand. Moreover, as reported by the same authors, features of the U=NAr bond are diversely modulated by the X ancillary ligand allowing stabilization of the metal (U^{IV}, U^{V} and U^{VI}) oxidation states.[39] The imide NAr donation ability during the reduction U^{V}/U^{IV} and oxidation U^{VI}/U^{V} processes is versatile, compensating either for the strong electron donating ketimide ligand or for the weak donating triflate one. Indeed, as can be noted in Table 3 for the triflate species, the global negative net charge for the imide NAr group changes from −0.92 to −1.19 *vs*. –0.68 during the reduction U^{V}/U^{IV} *vs*. oxidation U^{VI}/U^{V} process, indicating its high electron donation in this cases, compensating for the poor-electron donating triflate ancillary ligand. On the contrary, for the ketimide species, the NAr imide group exhibits

higher negative charges, passing from −0.99 to −1.26 *vs*. –0.88 during the reduction U^{V}/U^{IV} *vs*. oxidation U^{VI}/U^{V} process, respectively. These latter results confirm that a tuning of electron donation from the imide group is occurring according to the weak or strong charge transfer from the ancillary X ligand.

Bond order analyses were also performed using Mayer[71] and Nalewajski−Mrozek (NM)[72,73] methods (see the Computational Details), providing estimation of atom−atom bond orders that are particularly useful tools for structural inorganic and organometallic analyses.[74] Metal−ligand U–X and $U=N_{Ar}$ Mayer and Nalewajski−Mrozek (NM) bond orders for the three redox ($U^{VI}/U^{V}/U^{IV}$) species are reported in Table 4 (solvent effects taken into account). These bond orders vary following the same order as the ancillary ligand donating ability (OTf < SPh < C=CPh < Ph ~ Me ~ OPh < NPh_2 < $N=CPh_2$).[39] Indeed, considering the Mayer U−X bond orders of the neutral U^{V} complexes, it appears clearly that high values are observed for ancillary ligands leading to a significant U−X covalent bonding. The highest Mayer bond order value *i.e*. 1.255 is obtained for $N=CPh_2$ and the lowest one 0.435 for X = OTf in agreement with the expected high ionic character of the corresponding U−OTf bond. Considering the $U=N_{Ar}$ bond, it is interesting to note that the low σ−donation ability of the ancillary OTf ligand, is associated to high $U=N_{Ar}$ Mayer bond orders values (2.039/1.955/1.744) which traduce a high covalent character. Moreover, the Nalewajski−Mrozek analysis which includes electrostatic effects, lead to metal−imide $U=N_{Ar}$ higher bond orders equal to (2.590/2.759/2.784) for the three $U^{VI}/U^{V}/U^{IV}$ oxidation states, computed in solvated phase respectively with the OTf ligand. This is in the line with the evolution of the structural properties (Table 1) giving shorter $U=N_{Ar}$ bond distances (1.931/1.954/2.003 Å), revealing the crucial role of the imido group for both the oxidation U^{VI}/U^{V} and reduction U^{V}/U^{IV} faced to the triflate weak electron donor. In opposite, the strong $N=CPh_2$ σ/π−donor group towards the metal center $U^{VI}/U^{V}/U^{IV}$, leads to the lowest Mayer (1.915/1.815/1.611) and NM (2.526/2.582/2.478) bond orders as given in Table 3, correlating well with the longest $U=N_{Ar}$ bond distances (1.958/1.996/2.037 Å) as given in Table 1.

Table 4: ZORA/BP86/TZP Mayer and NM average bond orders of the $U^{VI}/U^{V}/U^{IV}$ $Cp_2U(=N-Ar)X$ complexes, in THF solution.

Ligand	U–X		U–N_{Ar}	
	Mayer	NM	Mayer	NM
OTf	0.611/0.414/0.306	1.548/1.346/1.153	2.039/1.901/1.744	2.590/2.739/2.784
C_6F_5	0.669/0.617/0.542	0.971/0.962/0.912	1.943/1.868/1.638	2.685/2.721/2.707
SPh	1.255/1.035/0.777	1.431/1.395/1.296	1.988/1.868/1.656	2.546/2.685/2.659
C=CPh	0.971/0.784/0.691	1.363/1.219/1.155	1.974/1.860/1.692	2.581/2.695/2.672
NPh_2	0.863/0.680/0.460	1.413/1.308/1.113	1.931/1.802/1.607	2.546/2.641/2.646
Ph	0.904/0.799/0.678	1.179/1.140/1.077	1.965/1.862/1.815	2.593/2.676/2.734
Me	0.936/0.814/0.662	1.662/1.620/1.539	1.995/1.862/1.588	2.617/2.734/2.655
OPh	0.976/0.824/0.634	1.739/1.659/1.507	1.944/1.818/1.603	2.546/2.650/2.624
$N(TMS)_2$	0.855/0.764/0.552	1.818/1.771/1.584	1.850/1.799/1.580	2.573/2.627/2.618
$N=CPh_2$	1.255/1.255/1.254	1.907/1.927/2.014	1.915/1.815/1.611	2.526/2.582/2.478

Interestingly, the U–X and U–N_{Ar} Mayer bond orders (Table 4) increase in the complexes with the oxidation state ($U^{VI} > U^{V} > U^{IV}$) as a result of the strong ligand-to-metal donation, enabling to stabilize efficiently the high oxidation states of the uranium complexes, in agreement with experimental trends.[35,39]

Redox properties

Ionization energies (IEs)

In order to study the oxidation process, we consider first the ionization energies (IEs) computed as difference between the Total Bonding Energies (TBEs) of the neutral U^{V} and cationic U^{VI} species at their optimized geometries (see Computational Details). The half−wave oxidation potentials $E_{1/2}$(V) from U^{VI}/U^{V} redox system (*vs.* $Cp_2Fe]^{+/0}$) have been measured.[38] Table 5 gives the computed TBEs and IEs, in the gas phase as well as in solution (THF) for all complexes, at the ZORA/BP86/TZP level of theory. The column (THF solvent effect and SO) gives the values of the IE taking into account solvent effects and spin–orbit coupling whereas the measured oxidation potentials $E_{1/2}$(V) are given in the last column.

Table 5: ZORA/BP86/TZP computed TBEs and IEs (eV) of the U^{VI}/U^{V} redox couple for the $Cp_2U(=N-Ar)(X)$ complexes in the gas phase, considering the THF solvent and including spin−orbit coupling (SO); and the experimental half−wave U^{VI}/U^{V} oxidation potentials $E_{1/2}$ (V) in the last column.

X	Gas phase			THF solvent			THF solvent + SO			$E_{1/2}$ (V)
	V	VI	IE	V	VI	IE	V	VI	IE	
OTf	–257.608	–250.933	6.675	–257.915	–252.709	5.206	–267.151	–261.899	5.252	**+0.36**
SPh	–320.748	–314.787	5.961	–320.933	–316.123	4.810	–330.195	–325.373	4.822	**0.00**
C=CPh	–332.219	–326.208	6.011	–332.399	–327.607	4.792	–341.645	–336.864	4.781	**–0.10**
Me	–264.523	258.384	6.146	–264.523	–259.830	4.683	–273.765	–269.067	4.698	**–0.13**
Ph	–315.595	–309.682	5.913	–315.753	–311.106	4.647	–325.007	–320.324	4.683	*na*[a]
OPh	–324.257	–318.245	6.012	–324.424	–319.747	4.677	–333.436	–328.857	4.579	**–0.22**
NPh_2	–395.798	–390.117	5.681	–395.993	–391.477	4.516	–405.248	–400.679	4.569	**–0.30**
$N=CPh_2$	–404.610	–398.738	5.872	–404.610	–400.074	4.536	–413.868	–409.359	4.509	**–0.34**

[a] *na:* not available

First, the gas phase calculation predicts the highest IE (6.675 eV) for the triflate U^{V} complex which is therefore the most difficult to oxidize, correlating well with the highest observed oxidation potential ($E_{1/2}$ = **+0.36** V). On the contrary, the ketimide ($N=CPh_2$) analogue exhibits the lowest IE (5.872 eV) probing to be the easiest to oxidize as indicated by the lowest half-wave oxidation potential ($E_{1/2}$ = **–0.34** V). In addition, solvation effects affect more importantly the cationic U^{VI} species than the neutral U^{V} one, leading to an energy increasing of *ca*. 1.5 *vs*. 0.2 eV, in their singlet and doublet state respectively, and an increase of IEs (1.2 eV on average). Spin–orbit coupling affects dramatically the TBE of the neutral and of the cationic species, but only slightly the IE (0.02 eV on average). This is mainly due to the local character of spin-orbit coupling leading to an approximate cancellation of their effects when subtracting the TBEs of the U^{VI} and of the U^{V} complexes.

Finally, a very nice linear regression (IEs *vs*. $E_{1/2}$) is obtained when including both solvent effects and the spin−orbit corrections, the R^2 correlation coefficient being equal to 0.98 (Figure 3). From this linear regression it is possible to estimate by interpolation the $E_{1/2}$ of a parent complex that has not yet been measured. Therefore, the half-wave oxidation potential of the Ph complex should be close to $E_{1/2}$ = –0.17 V its IE being computed equal to 4.683 eV as indicated on the Figure 3.

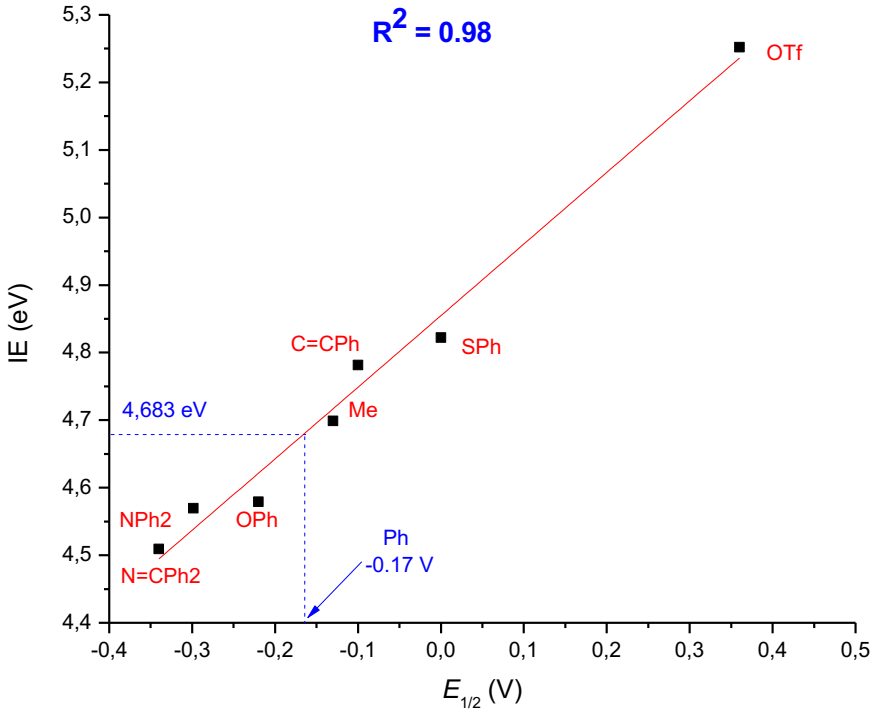

Figure 3: ZORA/BP86/TZP linear regression between ionization energies IEs(eV) and half−wave oxidation potential $E_{1/2}$(V) for the $Cp_2U(=N-Ar)X$ complexes (R^2 = 0.98 ; slope = 1.059) taking into account the THF solvent and spin−orbit effects.

It is interesting to note that taking into account the solvent effects but not spin-orbit corrections leads to the correlation factor (R^2 = 0.96), as shown on the figure S1 (in the SI). Moreover, neglecting solvation decreases even more importantly the IE−$E_{1/2}$ correlation coefficient (R^2 = 0.91).

Additionally, for two other ancillary ligands X, *i.e.* the electron attractor C_6F_5 and the electron donor $N(TMS)_2$ that we considered, the theoretical half-wave oxidation potential of their corresponding complexes should be close to $E_{1/2}$ = +0.24 and –0.26 V, respectively, their IEs being (Table S2) equal respectively to 5.098 and 4.570 eV, computed at the same level of theory (THF solvent + SO) as depicted on Figure S2.

Electron affinities (EAs)

The reduction of the neutral U^V $Cp_2U(=N-Ar)X$ complexes was studied first considering the electronic affinities (EAs) computed as the difference between the TBEs of the neutral U^V and anionic U^{IV} species at their optimized geometries. The computed TBEs and EAs, in the gas phase, in solution (THF) and including spin−orbit coupling, are given in Table 6. In the last column of this Table are displayed the measured half–wave reduction

potentials in volts ($-E_{1/2}$ *vs.* $[Cp_2Fe]^{+/0}$) of the neutral uranium(V) compounds, measured in THF.[39] Additionally, the energetic parameters, *i.e.*, the TBEs and EAs of the C_6F_5 and $N(TMS)_2$ model complexes are reported in the Table S3.

Table 6: ZORA/BP86/TZP computed TBEs (eV) and EAs (eV) of the U^V/U^{IV} redox couple for the $Cp_2U(=N-Ar)X$ complexes in the gas phase, in THF solution and including spin−orbit coupling (SO). Measured reduction potential $E_{1/2}$ (V) are given in the last column.

Structures X	Gas phase			THF solution			THF solution + SO			$E_{1/2}$ (V)
	V	IV	EA	V	IV	EA	V	IV	EA	
OTf	–257.608	–259.976	2.368	–257.915	–261.477	3.562	–267.151	–270.726	3.575	**–1.21**
SPh	–320.748	–322.816	2.068	–320.933	–324.306	3.373	–330.195	–333.575	3.380	**–1.43**
C=CPh	–332.219	–334.163	1.944	–332.399	–335.607	3.208	–341.645	–344.853	3.208	**–1.64**
NPh_2	–395.798	–397.689	1.891	–395.993	–399.153	3.160	–405.248	–408.416	3.168	**–1.65**
Ph	–315.595	–317.440	1.845	315.753	–318.820	3.067	–325.007	–328.172	3.165	*na*[a]
Me	–264.523	–266.332	1.809	–264.523	–267.679	3.156	–273.765	–276.900	3.135	**–1.71**
OPh	–324.257	–326.058	1.801	–324.424	–327.541	3.117	–333.436	–336.553	3.117	**–1.75**
$N=CPh_2$	–404.610	–406.401	1.791	–404.610	–407.594	2.984	–413.868	–416.884	3.016	**–1.84**

[a] *na:* not available

The triflate system, which has the lowest negative reduction potential (**−1.21** V) exhibits the highest EA (3.575 eV) as computed (THF solvent + SO), is the easiest to reduce. This is also true for the fluorinated electron-attractor C_6F_5 group, for which the predicted EA (3.397 eV) is high. On the contrary, the stronger σ/π−donor ketimide ($N=CPh_2$) congener exhibits the highest negative reduction potential (**−1.84** V) and the lowest EA (3.016 eV) being therefore the most difficult to reduce. The analogous strong electron donor $N(TMS)_2$ species exhibits a significantly low EA equal to 2.937 eV (Table S3).

These results are in agreement with experimental data reporting that the variation in reduction potential across the series (OTf, SPh, C=CpPh, OpPh, Me, Ph, NPh_2, $N=CPh_2$), is likely to derive from an interplay between pure electrostatic effects (*e.g.*, for the OTf and C_6F_5 complexes) and more covalent σ− and π−bonding interactions of ketimide and amide ($N=CPh_2$, $N(TMS)_2$), that shifts electron density to the metal center thereby affecting the reduction process.[39]

First, it is worth noting that the ordering of the reduction ability (EAs vs. $E_{1/2}$) of the U^{V} complexes is the same whatever the level of computation, *i.e.* gas, THF solvent and including spin−orbit coupling. Moreover, three ligands [Ph ~ Me ~ OPh][39] exhibit close σ/π−donating ability across the series, correlating well with the close electron affinities of the complexes (EAs = 3.165, 3.135, 3.117 eV). This electronic property is in good agreement with the observed reduction potential ($E_{1/2}$ = Me: **–1.71**, OPh: **–1.75** V); the experimental value of the Ph system being not available, it is estimated theoretically as $E_{1/2}$ = *–1.67* V *(vide infra*).

Considering the calculations performed in the gas phase, a linear regression appears between the computed EAs (gas) and measured $E_{1/2}$, the correlation coefficient R^2 being equal to 0.94 (slope = 0.946), as depicted on the Figure S3. Secondly, taking into account the solvent effects, the correlation depicted on Figure S4 is significantly better (R^2 = 0.98, slope = 0.873). Further introduction of spin−orbit coupling leads only to a slight improvement of the EA *vs* $E_{1/2}$ linear regression, namely that the correlation coefficient R^2 passes from the value 0.98 to 0.99 as depicted on the Figure 4. It is already seen from the computed EA values in Table 6 that variations less than 0.02 eV result from the spin-orbit coupling corrections.

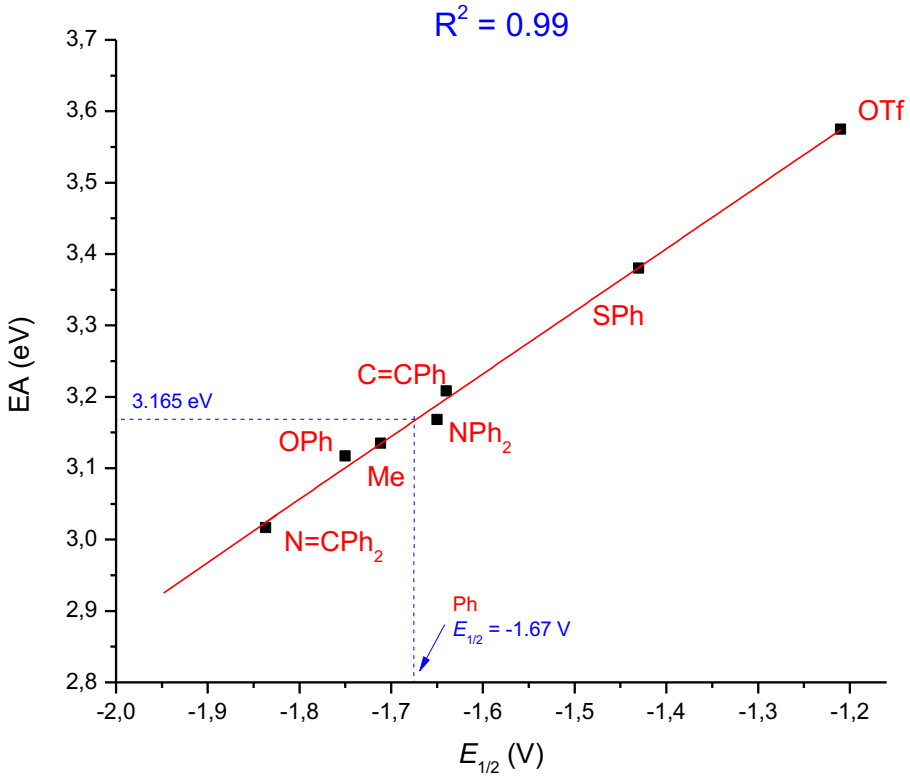

Figure 4: ZORA/BP86/TZP linear regression between electronic affinity EA(eV) computed in THF solution and including spin orbit effects, and measured reduction potential $E_{1/2}$(V) for the $Cp_2U(=N-Ar)X$ complexes ($R^2 = 0.99$: slope = 0.876).

The linear regression of Figure 4, permits to estimate for the X = Ph ligand, a reduction potential value of its complex of $E_{1/2} = -1.678$ V *vs*. EA equal to 3.165 eV. Similarly, the theoretical half-wave reduction potential of the two C_6F_5 and $N(TMS)_2$ species could be estimated considering their EAs equal to 3.397 *vs*. 2.937 (eV), respectively; the computations lead to $E_{1/2} = -1.413$ *vs.* −1.938 V for C_6F_5 and $N(TMS)_2$ respectively as shown on Figure S5. One can note that strong electron donors ligands *e.g*. X = $N(TMS)_2$ and $N=CPh_2$, lead to low electron affinity (EA) of the complexes correlating with a high negative reduction potential $E_{1/2}$. Indeed, the donating power of the ancillary X ligands OTf < SPh < C=CPh < [Ph ~ Me ~ OPh] < NPh_2 < $N=CPh_2$,[39] matches well with the computed EAs variation (Table 6). Furthermore, our results agree well with previous scalar relativistic BP86 calculations carried out by J. Kiplinger's group on the redox properties of the similar fluoroketimide U^{IV} complexes $Cp^*_2U(-N=CMeR)_2$ systems.[36] Their theoretical study leads to adiabatic EAs equal to 0.95 eV and 1.24 eV for R = 4–F–C_6H_4 and C_6F_5, respectively, whereas the corresponding $E_{1/2}$ are –2.64 and –2.34 V, showing that the complex exhibiting the highest EA is the easiest to reduce, in line with the greater electron–withdrawing property of the fluorinated phenyl group.

In order to correlate the variation of the half−wave redox potential $E_{1/2}$ to the frontier molecular orbitals *i.e*., the singly occupied molecular orbital SOMO(V) and the lowest unoccupied molecular orbital LUMO(V) of the neutral U^V species, we consider the energies (eV) of these frontier molecular orbitals (FMO), computed including solvent effects and spin–orbit coupling. In the Table 7, are also reported oxidation (U^{VI}/U^V) and reduction (U^V/U^{IV}) potential $E_{1/2}$ (V) for comparison with the FMO energies.

As shown in the Table 7, the LUMO energies of all U^V complexes are negative; this is indicative of the ability of these species to undergo a reduction process.

Table 7: ZORA/BP86/TZP LUMO/SOMO energies (eV) in THF solvent and spin−orbit effects included, of the U^V $Cp_2U(=N-Ar)X$ neutral complexes. Reduction (V/IV) and oxidation (V/VI) potentials $E_{1/2}$(Volts) and are given for comparison.

X	THF solvent + SO					
	LUMO	AE	$E_{1/2}$ (V/IV)	SOMO	IE	$E_{1/2}$ (VI/V)
OTf	−4.320	3.575	**–1.21**	−4.657	5.252	**+0.36**
C_6F_5	−4.128	3.397	*−1.41*	−4.440	5.098	*+0.14*
SPh	−4.087	3.380	**–1.43**	−4.319	4.822	**0.00**
C=CPh	−3.907	3.208	**–1.64**	−4.253	4.781	**–0.10**
Me	−3.829	3.168	**–1.65**	−4.182	4.698	**–0.13**
Ph	−3.858	3.165	*–1.67*	−4.133	4.683	*−0.17*
OPh	−3.767	3.135	**–1.71**	−4.036	4.579	**–0.22**
NPh_2	−3.886	3.117	**–1.75**	−4.004	4.569	**–0.30**
$N=CPh_2$	−3.712	3.016	**–1.84**	−4.003	4.570	**−0.32**
$N(TMS)_2$	−3.693	2.937	*−1.93*	−4.008	4.509	*–0.34*

Analyzing the plot of the LUMO(V) energy *vs*. the reduction potential variation as depicted in Figure 5, a very good correlation (R^2 = 0.99) is obtained the energies being computed in solution and including spin−orbit effects. One can note in Table 7, that the strong electron donating ketimide ($N=CPh_2$) ligand leads to a complex exhibiting a high LUMO(V) energy (–3.712 eV) for the neutral U^V species. In opposite, the weakest donor *i.e.,* the triflate (OTf) ligand exhibits the lowest LUMO(V) negative energy (–4.320 eV), correlating well with the half-wave reduction potential (–**1.84** *vs*. –**1.21** V). Similarly, the weak *vs*. strong electron donor C_6F_5 *vs*. $N(TMS)_2$ ligands, are predicted to lead to low *vs*. high LUMO(V) energy (–4.128 *vs*. –3.693 eV) of their complexes. Indeed, the ranking of the considered complexes, according to their reduction potential decreasing from the most donating ligand capacity to the lower one. Again, as given in the Table 6, this ranking correlates well with the increasing order of LUMO(V) energies: OTf < C_6F_5 < SPh < C=CPh < NPh_2 < Ph < Me < OPh < $N=CPh_2$ < $NTMS_2$, and suits also well their EA variation (Table 6).

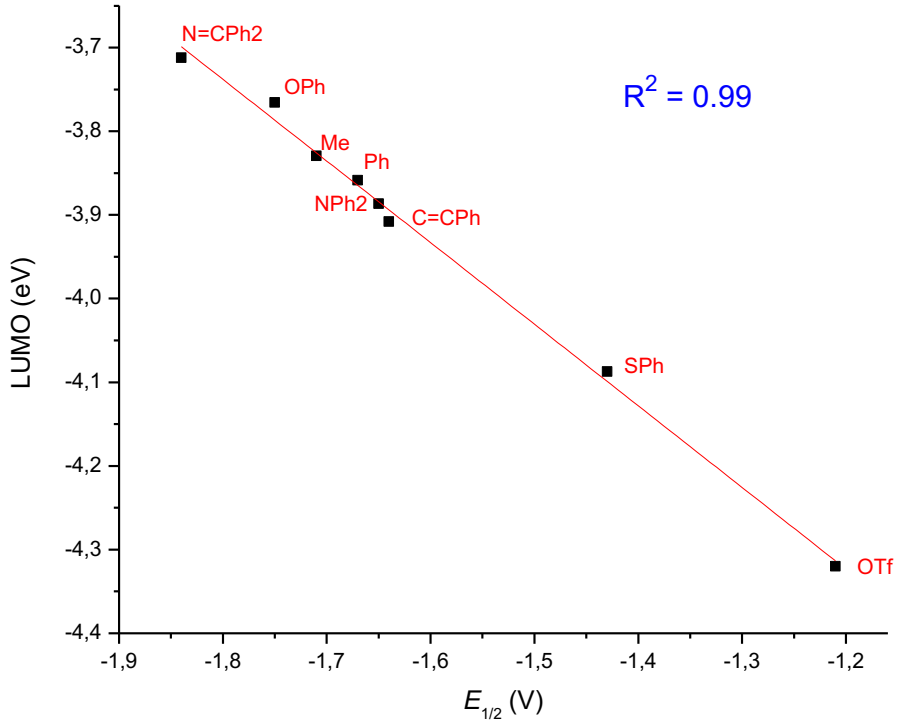

Figure 5: ZORA/BP86/TZP linear regression between LUMO energies (eV) and reduction potentials $E_{1/2}$(V) for the U^{V}/U^{IV} $Cp_2U(=N-Ar)X$ couple complexes (R^2 = 0.99, slope = –0.97). THF solvent and spin-orbit coupling effects included.

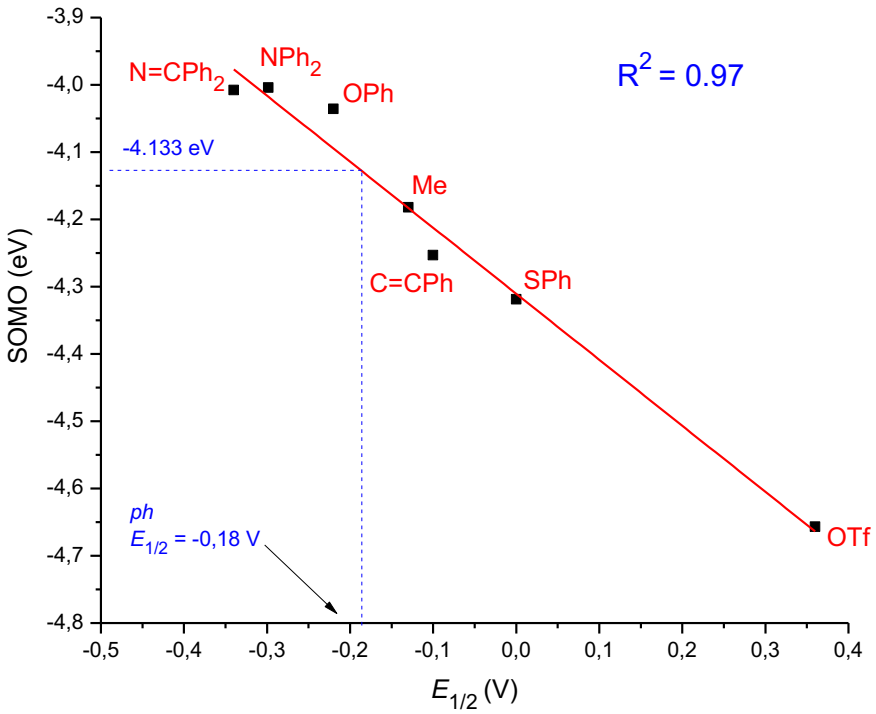

Figure 6: ZORA/BP86/TZP linear regression between **SOMO** energies (eV) and oxidation potentials $E_{1/2}$(V) for the U^{VI}/U^{V} $Cp_2U(=N-Ar)X$ couple complexes (R^2 = 0.97; slope = 1.059). THF solvent and spin−orbit coupling effects included.

Notably, as depicted on Figure 6 a rather good correlation (R^2 = 0.97) between computed SOMO energies and measured oxidation potential $E_{1/2}$(V) for the U^{VI}/U^{V} $Cp_2U(=N-Ar)X$ couple systems is obtained. As previously done using the computed IE, the oxidation potential $E_{1/2}$(V) for the three U^{VI}/U^{V} C_6F_5, Ph and $N(TMS)_2$ couple complexes for which no redox data exist, could be estimated using the linear regression. Considering their SOMO(V) energies respectively equal to –5.098, –4.133 and –4.003 (eV), the computations lead to $E_{1/2}$ = +0.14, –0.18 and. –0.32 V for C_6F_5, Ph and $N(TMS)_2$ respectively as shown in Figure S6. It is noteworthy, that the estimated oxidation potential ($E_{1/2}$ = +0.14 V) of the C_6F_5 group, correlates rather well with its strong electron withdrawing property.[36] Moreover, the SOMO(V) *vs*. $E_{1/2}(U^{VI}/U^{V})$ linear regression leads to the value of Ph oxidation potential ($E_{1/2}$ = −0.18 V), which is close to that obtained ($E_{1/2}$ = −0.17 V) from the IEs *vs*. $E_{1/2}(U^{VI}/U^{V})$ line. The two approaches lead to the same expected value of oxidation potential. The latter result relative to IEs was expected since the oxidation process involves predominantly 5f MOs (*vide infra*).

In this part, we study the effect of the substitution of the Cp* ligand of the real complexes by the Cp one in the computed systems. Although the nature of the Cp* ligands could affect the electronic structure and stability of the complexes, we expect that the trends observed using Cp will be conserved since the redox processes are rather local in character, involving only the $5f^n$ metallic orbitals. Indeed, the calculations including the solvent on three actual structures bearing the Cp* ligand namely the OTf, the Me and the ketimide complexes $(C_5Me_5)_2U(=N\text{-}Ar)(X)$ (X = OSO_2CF_3, Me and $N=CPh_2$), lead to EAs equal to 2.607, 2.747 and 3.157 eV, respectively, whereas the obtained values with Cp that are 2.984, 3.156 and 3.562 eV exhibit only a constant overestimation of ca. 0.4 eV relatively to the Cp* values. This result insures the same linear regression between the Cp * or Cp computed EA and the experimental values. Thus, the Cp* and Cp results agree, predicting the same EA ranking: ketimide < Me < OTf. In the same way, the computed IEs with Cp* including solvent are 4.178, 4.353 and 4.753 for the ketimide, Me and the triflate respectively, to be compared to the Cp values that are 4.536, 4.683 and 5.206 eV; the ranking of the IEs is the same, ketimide < Me < OTf.

To get a clearer vision on the FMO role on the redox properties, are displayed on Figure 7 the frontier MOs of the U^V complexes, *i.e.* the α-spin SOMOs and the LUMO. The percentages 6d/5f/Cp_2UNAr/X indicate the weights of the 6d and 5f metal orbitals as well as those of the metallic Cp_2UNAr moieties and ancillary X group in the MOs.

It can be seen that these frontier MOs are almost mainly uranium 5f orbitals with very small contribution from the ancillary X ligand. The X contribution to the LUMO is in overall zero, except for C=CPh, NPh_2, Ph and OPh reaching the maximum of 4.2% and no contribution of the imide (=N−Ar) group is observed. It is also interesting to note that the SOMO of the ketimide N=CPh_2 system differs significantly from the other MOs. Notably, its 5f orbital contribution (72.3%) to the SOMO in such U^V system is the lowest relatively to the other species. This correlates well with the lowest 5f spin orbital population reported for this species (Table 2).

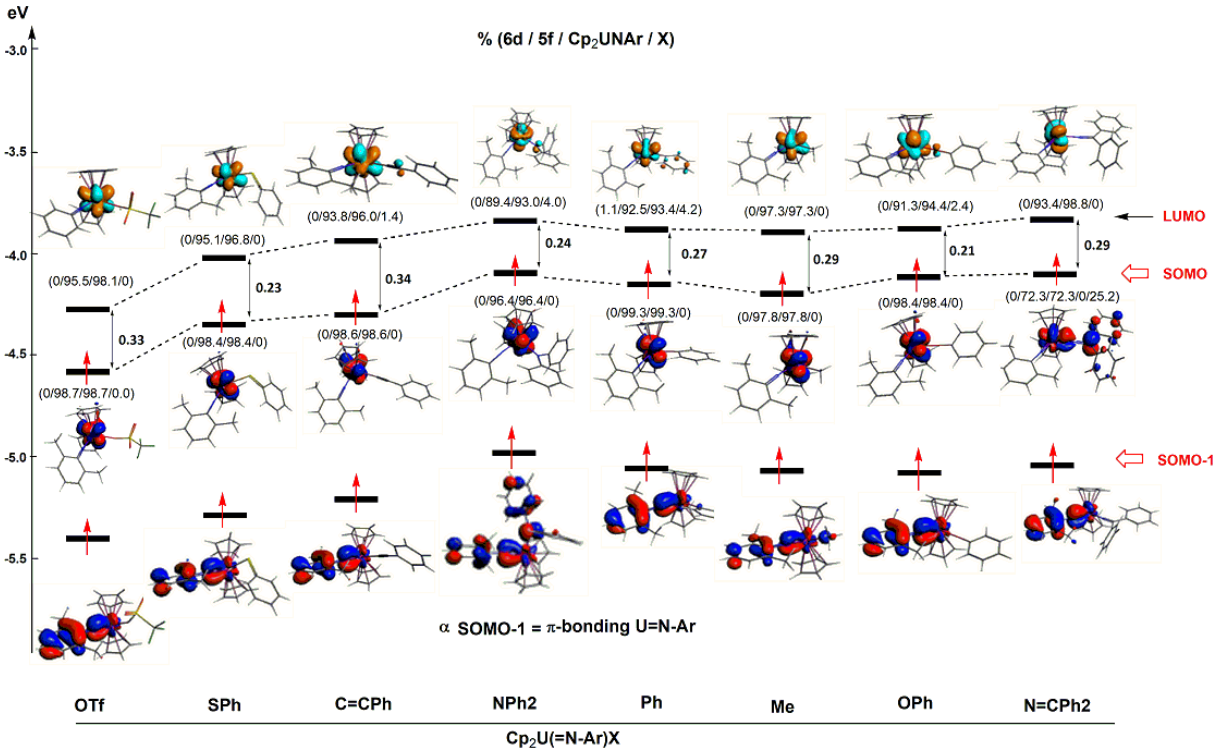

Figure 7: Frontier α−MO diagram of the neutral U^V Cp_2U(=N−Ar)X complexes in solvated (THF) phase at the ZORA/BP86/TZP level. The dots connect the LUMO/SOMO energy levels.

The LUMO(V) of the neutral complexes is formally populated upon reduction. The energy variation of this orbital suits the electron withdrawing character of the ancillary X ligand;

higher this character, more the LUMO(V) is stabilized and the reduction process easier to make. It is the case for the OTf ligand for instance. On the contrary, the $Cp_2U(=N-Ar)X$ complex, with X= $N=CPh_2$ strong electron donor, is difficult to reduce, its LUMO is not stabilized. As can be seen in this MO diagram (Figure 7), the LUMO(V) energies follow the order: OTf < SPh < C=CPh < OPh < Me < Ph < NPh_2 < $N=CPh_2$, in agreement with the computed electron donating capacity of X.[39] A similar trend is observed regarding the ionization of the complexes, strong electron donors ancillary ligands will lead to a destabilization of the SOMO(V) (Figure 7) thus to an easier oxidation.

Conclusions

The redox behavior of a series of biscyclopentadienyl imido-uranium(V) complexes $Cp_2U(=N-Ar)X$ (Ar = 2,6-Me_2-C_6H_3 ; X = OTf, SPh, C=CPh, OPh, Me, Ph, NPh_2, $N=CPh_2$, C_6F_5, $N(TMS)_2$) has been investigated for the first time, at the relativistic ZORA/BP86/TZP computations taking into account solvent (THF) effects employing the COSMO solvation model and taking into account spin−orbit coupling. Our study confirms that this computational methodology is accurate enough. Indeed, very good linear correlations have been obtained (R^2 = 0.98) between the computed ionization energies (IE) and the experimental half−wave oxidation potentials and also between the computed electron affinities (EA) and the measured electrochemical reduction potentials (R^2 = 0.99). The study brings to light the importance of solvation effects that must be considered in order to achieve a good agreement between theory and experiment, whereas introducing spin-orbit coupling corrections led only to a slight improvement of this agreement. It is seen in Table S4 that the SO effects induce a slight stabilization of the FMO less than 0.1 eV.

Investigation of the structural and electronic properties, considering metal−ligand Mayer/Nalewajski−Mrozek bond orders and MO analyses, allowed to understand the evolution of the computed IE and EA with the nature of the ancillary X ligand. Our results reveal a tight relationship between the variation in metal−ligand U–X and $U=N_{Ar}$ bond distances and the redox potential ($-E_{1/2}$) which is attributed to a subtle interplay between purely electrostatic effects (e.g., OTf) and more pronounced covalent σ- and π-bonding interactions (e.g., ketimide $N=CPh_2$). Moreover, the LUMO(V) energies of neutral U^V species, increase with the electron donating strength of X according to OTf < SPh < C=CPh < NPh_2 < Ph < Me < OPh <$N=CPh_2$, and suit also well with their EA variation and reduction potentials $E_{1/2}$.

Moreover, our study revealed the crucial role of the imide NAr group whose is versatile accordingly to the strength of the electron transfer from the ketimide ($N{=}CPh_2$) and triflate (OTf) ancillary X ligands.

Finally, our computational methodology was used to predict the redox half wave potentials for the U^V complexes bearing the phenyl, C_6F_5 and $N(TMS)_2$ ancillary ligands, that have not yet been measured. Of course, any actinide complex, especially those exhibiting hazardous character could be computed that way.

Computational Details

Determination of electron affinities (EA) is challenging,[52,53] and since measured EAs are largely adiabatic, the most direct theoretical method is to calculate EA as the difference (ΔE) of the energies of the neutral and anionic forms of the neutral complexes at their respective optimized geometries.[4,22] In the same way, ionisation energies (IEs) are obtained as the difference between the energies of the cationic and neutral forms (*vide infra*).

The calculations were performed using Density Functional Theory (DFT),[75] using the Amsterdam Density Functional (ADF2019.302) release program package.[76] with scalar relativistic corrections being introduced via the Zero Order Regular Approximation (ZORA)[77,78] and at spin unrestricted framework as the systems under consideration are $5f^n$ open-shell. Solvents effects have been taken into account using the Conductor–like Screening Model for Realistic Solvents (COSMO–RS).[79] These ZORA/DFT calculations were performed using the Vosko–Wilk–Nusair functional (VWN)[80] for the local density approximation (LDA) and the gradient corrections for exchange and correlation of Becke and Perdew,[81,82] respectively, i.e. the BP86 functional, have been used. Triple–ζ Slater–type valence orbitals (STO) augmented by one set of polarization functions were used for all atoms. For all elements, the basis sets were taken from the ADF/ZORA/TZP database. The more extended ZORA/TZ2P basis set has also been used to check the accuracy of the computed properties. The 'small' frozen–core approximation, where the core density is obtained from four–component Dirac–Slater calculations, has been applied for all atoms. 1s core electrons were frozen respectively for boron B[1s], carbon C[1s] and oxygen O[1s]. For sulphur S[2p] and chlorine Cl[2p], the 1s/2s/2p cores were frozen. The U[5d] valence space of the heavy element includes the 5f/6s/6p/6d/7s/7p shells (14 valence electrons). Several studies have shown that the ZORA/BP86/TZP approach reproduces the experimental geometries and ground states properties of f–element compounds with a satisfying accuracy.[52-59,61,62] In our

case, we carried out first the full geometry optimizations of the species under consideration, in the gas phase, at the spin unrestricted level. Next, the geometries were re−optimized in the THF solvent using the COSMO model. We used the Klamt et al.[83,84] framework and non–default Delley type of cavity,[85] the solvent effect being simulated with its dielectric constant of 7.58 and a radius of 3.18 Å. Then, single point calculations including spin–orbit corrections were carried out and based on the previously optimized geometries, for both the gas and solvated phases.

For all $Cp_2U(=N-Ar))X$ complexes under consideration, we considered the highest spin state as the most stable ground state configuration, *i.e.*, doublet ($5f^1$) spin states for the neutral U^V species and triplet ($5f^2$) for the U^{IV} anionic ones. Spin contaminations were checked in all cases (comparison between the computed values of the squared spin operator $\langle S^2 \rangle$ and exact values showed deviations less than 3 %)

The ADF program that we use produces total bonding energies (TBE) rather than total energies, so that in terms of the TBE obtained at optimized geometries, EA and ionization energy (IE) are computed as follows:

EA = TBE(neutral) –TBE(anion) = TBE(U^V) – TBE(U^{IV}) for the reduction process

IE = TBE(cation) – TBE(neutral) = TBE(U^{VI}) – TBE(U^V) for the oxidation process

The computation of accurate values of half-wave reduction or oxidation potentials is rather challenging and should include the solvated electron.[54] Neglecting this important factor will only add a constant factor to the energy differences that we compute. This will not affect the correlations between theoretical and experimental values that we consider.

As the ADF program permits an energy decomposition into chemically useful terms,[86-88] we carried out spin-unrestricted fragment calculations considering the following molecular moieties in interaction, Cp_2U, NAr and X in order to get the charges borne by these fragments, for the different oxidation states U^{IV}, U^V and U^{VI} of the metal.

Molecular geometries and molecular orbital plots were generated using the ADF-GUI programs.[76]

Acknowledgements

We acknowledge the Algerian PRFU project funding (2018−2022: Grant No. B00L01UN250120180015) and the French GENCI IDRIS and GENCI CINES for an allocation of computing time (Grant No. 2018−2019−080649).

References

1. Edelmann, F. T. Lanthanides and actinides: Annual survey of their organometallic chemistry covering the year 2018. *Coord. Chem. Rev*. **2019**, *398*, 113005.
2. Boucekkine, A.; Belkhiri, L. f−Element Complexes. In: Jan Reedijk and Kenneth Poeppelmeier, Editors. Comprehensive Inorganic Chemistry II, Vol 9. Oxford: Elsevier; **2013**, pp. 277−319.
3. Refn, V. E.; Kubus, M.; Mossin, S.; R. Larsen, W.; K. Pedersen, S. A Redox−Innocent Uranium(IV)−Quinoid Metal−Organic Framework. *ACS Omega* **2020**, *5*, 3462−3466.
4. McSkimming, A.; Su, J.; Cheisson, T.; Gau, M. R.; Carroll, P. J.; Batista, E. R.; Yang, P.; Schelter, E. J. Coordination Chemistry of a Strongly−Donating Hydroxylamine with Early Actinides: An Investigation of Redox Properties and Electronic Structure. *Inorg. Chem*. **2018**, 57, 4387−4394.
5. Arumugam, K.; Burton, N. A. Uranyl-Bound Tetra-Dentate Non-Innocent Ligands: Prediction of Structure and Redox Behaviour Using Density Functional Theory. *Chem. Phys. Chem.* **2019**, *20*, 1869−1878.
6. Arumugam, K.; Burton. N. A. Density functional theory (DFT) calculations of VI/V reduction potentials of uranyl coordination complexes in non−aqueous solutions. *Phys. Chem. Chem. Phys*. **2019**, *21*, 3227−3241.
7. Tsoureas, N.; Cloke, F. G. N. Mixed sandwich imido complexes of Uranium(V) and Uranium(IV): Synthesis, structure and redox behavior. *J. Organomet. Chem*. **2018,** *857*, 25−33.
8. Khungar, B.; Roy, A.; Kumar, A.; Sadhu, B.; Sundararajan, M. Predicting the redox properties of uranyl complexes using electronic structure calculations. *Int. J. Quant. Chem*. **2017**, *117*, e25370.

9. Natrajan, L. S.; Swinburne, A. N.; Andrews, M. B.; Randall, S.; Heath, S. L. Redox and environmentally relevant aspects of actinide(IV) coordination chemistry, *Coord. Chem. Rev*. **2014**, *266*, 171−193.
10. Steele, H. M.; Guillaumont, D.; Moisy, P. Density Functional Theory Calculations of the Redox Potentials of Actinide(VI)/Actinide(V) Couple in Water. *J. Phys. Chem.* A **2013**, *117*, 4500–4505.
11. Kias, F.; Talbi, F.; Elkechai, A.; Boucekkine, A.; Hauchard, D.; Berthet, J.−C.; Ephritikhine. M. Redox Properties of Monocyclooctatetraenyl Uranium(IV) and (V) Complexes: Experimental and Relativistic DFT Studies. *Organometallics* **2017**, *36*, 19, 3841–3853.
12. Boreen, M. A.; Lussier, D. J.; Skeel, B. A.; Lohrey, T. D.; Watt, F. A.; Shuh, D. K.; Long, J. R.; Hohloch, S.; Arnold, J. Structural, Electrochemical, and Magnetic Studies of Bulky Uranium(III) and Uranium(IV) Metallocenes. *Inorg. Chem*. **2019**, *58*, 16629–16641.
13. Niu, S.; Cai, H.-X.; Zhao, H.-B.; Li, L.; L. Pan. Q.-J. Redox and structural properties of accessible actinide(II) metallocalixarenes (Ac to Pu): a relativistic DFT study. *RSC Adv*. **2020**, *10*, 26880–26887
14. Pagano, J.K.; Erickson, K.A.; Scott, B.L.; Morris, D.E.; Waterman, R.; Kiplinger, J.L. Synthesis and characterization of a new and electronically unusual uranium metallacyclocumulene, $(C_5Me_5)_2U(\eta^4-1,2,3,4-PhC_4Ph)$, *J. Organomet. Chem*. **2017**, *829*, 79−84.
15. Erickson, K.A.; Kagan, B.D.; Scott, B.L.; Morris, D.E.; Kiplinger, J.L. Revisiting the bis(dimethylamido) metallocene complexes of thorium and uranium: improved syntheses, structure, spectroscopy, and redox energetics of $(C_5Me_5)_2An(NMe_2)_2$ (An = Th, U). *Dalton Trans*. **2017**, *46*, 11208-11213.
16. Lichtscheidl, A.G.; Pagano, J.K.; Scott, B.L.; Nelson, A.T.; Kiplinger, J.L. Expanding the chemistry of actinide metallocene bromides. synthesis, properties and molecular structures of the tetravalent and trivalent uranium bromide complexes: $(C_5Me_4R)_2UBr_2$, $(C_5Me_4R)_2U(O\text{-}2,6\text{-}^iPr_2C_6H_3)(Br)$, and $[K(THF)][(C_5Me_4R)_2UBr_2]$ (R = Me, Et). *Inorganics* **2016**, *4*, 1.
17. Hayton T. W. Recent developments in actinide–ligand multiple bonding. *Chem. Commun*. **2013**, *49*, 2956-2973.

18. Hayton T.W.; Kaltsoyannis N. Organometallic Actinide Complexes with Novel Oxidation States and Ligand Types. Experimental and Theoretical Approaches to Actinide Chemistry. Eds; John Wiley & Sons Ltd. **2018**, pages 181–236.
19. Neidig, M.L.; Clark, D.L.; Martin, R.L. Covalency in f−element complexes. *Coord. Chem. Rev*. **2013**, *257*, 394–406.
20. Jung, J.; Atanasov, M.; Neese, F. Ab Initio Ligand−Field Theory Analysis and Covalency Trends in Actinide and Lanthanide Free Ions and Octahedral Complexes. *Inorg. Chem*. **2017**, *56*, 8802–8816.
21. Lu, E.; Sajjad, S.; Berryman, V.E.J.; Wooles, A. J.; Kaltsoyannis, N.; Liddle, S. T. Emergence of the structure−directing role of f−orbital overlap−driven covalency. *Nat. Commun*. **2019**, 10, 634.
22. Arumugam, K.; Becker, U. Computational Redox Potential Predictions: Applications to Inorganic and Organic Aqueous Complexes, and Complexes Adsorbed to Mineral Surfaces. *Minerals* **2014**, *4*, 345−387.
23. Dam, H. H.; Reinhoudt, D. N.; Verboom, W. Multicoordinate ligands for actinide/lanthanide separations. *Chem. Soc. Rev*. **2007**, *36*, 367−377.
24. Wu, Q.-Y.; Lan, J.-H.; Wang, C.-Z.; Cheng, Z.-P.; Chai, Z.-F.; Gibson, J. K.; Shi, W.-Q. Paving the way for the synthesis of a series of divalent actinide complexes: a theoretical perspective. *Dalton Trans*. **2016**, *45*, 3102–3110.
25. Murillo, J.; Skye, F. Organometallic Chemistry of Pentavalent Uranium. *The Heaviest Metals: Science and Technology of the Actinides and Beyond*, **2019**, *1(4)*, 263.
26. Andrea, T.; Eisen, M. S. Recent advances in organothorium and organouranium catalysis. *Chem. Soc. Rev*. **2008**, *37*, 550−567.
27. Spencer, L. P.; Gdula, R. L.; Hayton, T. W.; Scott, B.L.; Boncella, J. M. Synthesis and reactivity of bis(imido) uranium(VI) cyclopentadienyl complexes. *Chem. Commun*. **2008**, 4986−4988.
28. Weiss, C. J.; Marks, T. J. Organo−f−element catalysts for efficient and highly selective hydroalkoxylation and hydrothiolation, *Dalton Trans*. **2010**, *39*, 6576−6588.
29. T. W. Hayton, Metal–ligand multiple bonding in uranium: structure and reactivity. *Dalton Trans*. **2010**, *39*, 1145−1158.
30. Sharma, M.; Eisen, M. S. Metallocene Organoactinide Complexes. *Struct. Bond.* **2008**, *127*, 1–85.

31. Kiernicki, J. J.; Staun, S. L.; Zeller, M.; Bart, S. C. A Uranium(IV) Triamide Species with Brønsted Basic Ligand Character: Metal–Ligand Cooperativity in the f Block. *Organometallics* **2017**, *36*, 665−672.
32. Boreen, M. A;. McCabe, K. N.; Lohrey, T. D.; Watt, F. A.; Maron, L.; Hohloch, S.; Arnold, J. Uranium Metallocene Azides, Isocyanates, and Their Borane-Capped Lewis Adducts. *Inorg. Chem*. **2020**, 59, 8580−8588.
33. Boreen, M. A.; Groß, O. A.; Hohloch, S.; Arnold, J. Isocyanide adducts of tri- and tetravalent uranium metallocenes supported by tetra(isopropyl)cyclopentadienyl ligands. *Dalton. Trans*. **2020**, 49, 11971−11977.
34. Kiplinger, J. L.; John, K. D.; Morris, D. E.; Scott, B. L.; Burns, C. J. $[(C_5Me_5)_2U(Me)(OTf)]_2$: A New Reagent for Uranium Metallocene Chemistry. Preparation of the First Actinide Hydrazonato Complexes. *Organometallics* **2002**, *21*, 21, 4306–4308.
35. Morris, D. E. Da Re, R. E.; Jantunen, K. C.; Castro−Rodriguez, I.; Kiplinger, J. L. Trends in Electronic Structure and Redox Energetics for Early−Actinide Pentamethylcyclopentadienyl Complexes, *Organometallics* **2004**, *23*, 5142−5153.
36. Schelter, E. J.; Yang, P.; Scott, B. L.; Thomson, J. D.; Martin, R. L.; Hay, P. J.; Morris, D. E.; Kiplinger, J. J. Systematic Studies of Early Actinide Complexes: Uranium(IV) Fluoroketimides. *Inorg. Chem*. **2007**, *546*, 7477−7488.
37. Graves, C. R.; Schelter, E. J.; Cantat, T.; Scott, B. L.; Kiplinger, J. L. A Mild Protocol To Generate Uranium(IV) Mixed−Ligand Metallocene Complexes using Copper(I) Iodide. *Organometallics* **2008**, *27*, 5371–5378.
38. Graves, C. R.; Scott, B. L.; Morris, D. E.; Kiplinger, J. L. Tetravalent and Pentavalent Uranium Acetylide Complexes Prepared by Oxidative Functionalization with CuC=CPh. *Organometallics* **2008**, *27*, 3335–3337.
39. Graves, C. R.; Vaughn, A. E.; Schelter, E. J.; Scott, B. L.; Thompson, J. D.; Morris, D. E.; Kiplinger, J. L. Probing the Chemistry, Electronic Structure and Redox Energetics in Organometallic Pentavalent Uranium Complexes. *Inorg. Chem*. **2008**, *47*, 11879−11891.
40. Graves, C. R.; Yang, P.; Kozimor, S. A;. Vaughn, A. E.; Clark, D. L.; Conradson, S. D.; Schelter, E. J.; Scott, B. L. Organometallic Uranium(V)−Imido Halide Complexes: From Synthesis to Electronic Structure and Bonding *J. Am. Chem. Soc*. **2008**, *130*, 5272–5285.

41. Thomson, R. K.; Scott, B. L.; Morris, D. E.; Kiplinger, J. L. Synthesis, structure, spectroscopy and redox energetics of a series of uranium(IV) mixed−ligand metallocene complexes. *C. R. Chimie* **2010**, *13*, 790−802,

42. Thomson, R.K.; Graves, C.R.; Scott, B.L.; Kiplinger. J. L. Synthesis and Molecular Structure of $(C_5Me_5)_2U(O^tBu)(SePh)$: A Mixed-Ligand Alkoxide-Selenide Uranium(IV) Metallocene Complex Resulting from *tert*-Butoxy-Trimethylsilane Elimination. *J. Chem. Crystallogr*. **2011**, *41*, 1241-1244.

43. Thomson, R. K.; Graves, C. R.; Scott, B. L.; Kiplinger. J. L. Uncovering alternate reaction pathways to access uranium(IV) mixed-ligand aryloxide–chloride and alkoxide–chloride metallocene complexes: Synthesis and molecular structures of $(C_5Me_5)_2U(O\text{-}2,6\text{-}^iPr_2C_6H_3)(Cl)$ and $(C_5Me_5)_2U(O\text{–}^tBu)(Cl)$. *Inorg. Chim. Acta* **2011**, *369*, 270-273.

44. Hauchard, D.; Cassir, M.; Chivot, J.; Ephritikhine, M., Electrochemical study of uranium(IV) and uranium(IV) organometallic compounds in tetrahydrofuran by means of conventional microelectrodes and ultramicroelectrodes: Part I. Application to the Na(Hg) reduction of Cp_3UCl (Cp = η^5−C_5H_5). *J. Electroanal. Chem*. **1991**, *313*, 227−241.

45. Hauchard, D.; Cassir, M.; Chivot, J.; Baudry, D.; Ephritikhine, M. Electrochemical study of uranium (IV) and (III) organometallic compounds in tetrahydrofuran by means of conventional microelectrodes and ultramicroelectrodes: Part II. Application to borohydride compounds—study of the stability of $Cp_2U(BH_4)_2$. *J. Electroanal. Chem*. **1993**, *347*, 399−407.

46. Clappe, C.; Leveugle, D.; Hauchard, D.; Durand, G. Electrochemical studies of tricyclopentadienyl uranium IV chloride complexes: $(RCp)_3UCl$ ($RCp=RC_5H_4$ with R=H; Me: CH_3; tBu: $(CH_3)_3C$); TMS: $(CH_3)_3Si$): Evidence of a disproportionation mechanism in oxidation. *J. Electroanal. Chem*. **1998**, *448*, 95−103.

47. Sonnenberger, D.C.; Gaudiello, J.G. Cyclic voltammetric study of organoactinide compounds of uranium(IV) and neptunium(IV). Ligand effects on the M(IV)/M(III) couple. *Inorg. Chem*. **1988**, *27*, 2747−2748.

48. Ossola, F.; Zanella, P.; Ugo, P.; Seeber, R. Electrochemical study of triscyclopentadienyl uranium complexes. *Inorg. Chim. Acta* **1988**, *147*, 123−126.

49. Schnabel, R.C.; Scott, B.L.; Smith, W.H.; Burns, C.J. Synthesis and structural characterization of uranium ansa−metallocene complexes containing organoimido

functional groups; electronic effects of ancillary ligands. *J. Organomet. Chem*. **1999**, *591,* 14−23.

50. Berthet, J. C.; Thuéry, P.; Ephritikhine, M. Advances in f−element cyanide chemistry. *Dalton Trans*. **2015**, *44*, 7727–7742.
51. Ephritikhine, M. Molecular actinide compounds with soft chalcogen ligands. *Coord. Chem. Rev.* **2016**, *319*, 35–62.
52. Rienstra−Kiracofe, J. C.; Tschumper, G. S.; Schaefer, H. F.; Nandi, S.; Ellison, G.B. Atomic and Molecular Electron Affinities: Photoelectron Experiments and Theoretical Computations. *Chem. Rev.* **2002**, *102*, 231−282.
53. Bateni, S. B.; England, K. R.; Galatti, A. T.; Kaur, H.; Mendiola, V. A.; Mitchell, A. R.; Vu, M. H.; Gherman, B. F.; Miranda, J. A. Prediction of reduction potentials from calculated electron affinities for metal-salen compounds. *Beilstein J. Org. Chem*. **2009**, *5*, No. 82.
54. Roy, L. E.; Jakubikova, E.; Guthrie, M. G.; Batista, E. R. Calculation of One-Electron Redox Potentials Revisited. Is It Possible to Calculate Accurate Potentials with Density Functional Methods? *J. Phys. Chem. A* **2009**, *113*, 6745–6750.
55. Reta, D.; Ortu, F.; Randall, S.; Mills, D. P.; Chilton, N. F.; Winpenny, R. E.P.; Natrajan, L.; Edwards, B.; Kaltsoyannis, N. The performance of density functional theory for the description of ground and excited state properties of inorganic and organometallic uranium compounds. *J. Organomet. Chem*. **2018**, *857*, 58–74.
56. Elkechai, A.; Meskaldji, S.; Boucekkine, A.; Belkhiri, L.; Bouchet, D.; Amarouche, M.; Clappe, C.; Hauchard, D.; Ephritikhine, M. A relativistic DFT study of the electron affinity of the biscyclopentadienyl uranium complexes $Cp*_2UX_2$. *J. Mol. Struct. theochem* **2010**, *954*, 115−123.
57. Elkechai, A.; Boucekkine, A.; Belkhiri, L.; Hauchard, D.; Clappe, C.; Ephritikhine, M. Electron affinities of biscyclopentadienyl and phospholyl uranium(IV) borohydride complexes: Experimental and DFT studies. *C. R. Chimie* **2010**, *13*, 860−869.
58. Elkechai, A.; Boucekkine, A.; Belkhiri, L.; Amarouche, M.; Clappe, C.; Hauchard, D.; Ephritikhine, M. A DFT and experimental investigation of the electron affinity of the triscyclopentadienyl uranium complexes Cp_3UX. *Dalton Trans.* **2009**, 2843−2849.
59. Elkechai, A.; Kias, F.; Talbi, F.; Boucekkine, A. R Redox properties of biscyclopentadienyl uranium(V) imido-halide complexes: a relativistic DFT study. *J. Mol. Model*. **2014**, *20*, 2294.

60. Lobach, A.S.; Strelets, V. V. Relationship between reduction potentials and electron affinities of fullerenes and their derivatives. *Russ. Chem. Bull., Int. Ed*. **2001**, *50*, 1516−1518.
61. Talbi−Ingrachen, F.; Talbi, F.; Kias, F.; Elkechai, A.; Boucekkine, A.; Daul, C. DFT investigation of methane metathesis with L_2AnCH_3 actinide complexes catalysts (L = Cl, Cp, Cp*; An = Ac, Th, Pa, U, Np, Pu). *Comp. Theo. Chem.* **2018**, *1138*, 123−134.
62. Talbi, F.; Castro, L.; Kias, F.; Elkechai, A.; Boucekkine, A.; Ephritikhine, M. Theoretical investigation of the reactivity of bispentamethylcyclopentadienyl uranium(IV) bisthiolate complexes with the heteroallene molecules CS_2 and CO_2. *J. Organomet. Chem*. **2019**, *901*, 120947.
63. Shannon, R.D. Revised effective ionic radii and systematic studies of interatomic distances in halides and chalcogenides. *Acta Crystallogr*. *A* **1976**, *32*, 751
64. Lewis, A. J.; Mullane, K. C.; Nakamaru-Ogiso, E.; Carroll, P. J.; Schelter, E. J. The Inverse Trans Influence in a Family of Pentavalent Uranium Complexes. *Inorg. Chem*. **2014**, *53*, 6944−6953.
65. Lewis, A.J.; Carroll, P. J.; Schelter, E. J. Stable Uranium(VI) Methyl and Acetylide Complexes and the Elucidation of an Inverse Trans Influence Ligand Series. *J. Am. Chem. Soc*. **2013**, *135*, 13185−13192.
66. R.S. Mulliken, Electronic Population Analysis on LCAO−MO Molecular Wave Functions. I. *J. Chem. Phys.* **1955**, *23*, 1833−1840.
67. Reed, A.E.; Curtiss, L.A.; Weinhold, F. Intermolecular interactions from a natural bond orbital, donor−acceptor viewpoint. *Chem. Rev.* **1988**, *88*, 899−926.
68. Wu, H.; Wu, Q.Y.; Wang, C.Z.; Lan, J.H.; Liu, Z.R.; Chai, Z.F.; Shi, W.Q. New insights into the selectivity of four 1,10−phenanthroline−derived ligands toward the separation of trivalent actinides and lanthanides: a DFT based comparison study. *Dalton Trans. Int. Ed.* **2016**, *45*, 8107−8117.
69. Hirshfeld, F.L. Bonded-atom fragments for describing molecular charge densities. *Theor. Chim. Acta* **1977**, *44*, 129.
70. Fonseca Guerra, C.; Handgraaf, J.W.; Baerends, E.J.; Bickelhaupt, F.M. Voronoi deformation density (VDD) charges: Assessment of the Mulliken, Bader, Hirshfeld, Weinhold, and VDD methods for charge analysis. *J. Comput. Chem.* **2004**, *25*, 189–210
71. Mayer, I. Charge, bond order and valence in the ab initio SCF theory. *Chem. Phys. Lett.* **1983**, *97*, 270−274.

72. Nalewajski, R.F.; Mrozek, J. Modified valence indices from the two−particle density matrix. *Int. J. Quant. Chem*. **1994**, *51*, 187−200.
73. Nalewajski, R.F.; Mrozek, J.; Michalak, A. Two−electron valence indices from the Kohn−Sham orbitals. *Int. J. Quant. Chem*. **1997**, *61*, 589−601.
74. Michalak, A.; Dekock, R.; Ziegler, T. Bond Multiplicity in Transition−Metal Complexes: Applications of Two−Electron Valence Indices. *J. Phys. Chem. A* **2008**, *112*, 7256−7263.
75. te Velde, G.; Bickelhaupt, F.M.; Baerends, E.J.; Fonseca Guerra, C.; van Gisbergen, S.J.A.; Snijder, J.G.; Ziegler, T. Chemistry with ADF. *J. Comput. Chem*. **2001**, *22*, 931−967.
76. ADF 2019.302, SCM, Theoretical Chemistry, Vrije Universiteit, Amsterdam, The Netherlands, http://www.scm.com.
77. van Lenthe, E.; Baerends, E.J.; Snijders, J.G. Relativistic regular two−component Hamiltonians. *J. Chem. Phys*. **1993**, *99*, 4597−4610.
78. van Lenthe, E.; Ehlers, A.E.; Baerends, E.J. Geometry optimization in the Zero Order Regular Approximation for relativistic effects, *J. Chem. Phys*. **1999**, *110*, 8943−8953.
79. Pye, C.; Ziegler, T. An implementation of the conductor−like screening model of solvation within the Amsterdam density functional package. *Theor. Chem. Acc*. **1999**, *101*, 396–408.
80. Vosko, S.D.; Wilk L.; Nusair, M. Accurate spin-dependent electron liquid correlation energies for local spin density calculations: a critical analysis. *Can. J. Chem*. **1980**, *58*, 1200−1211.
81. Becke, A.D. Density−functional exchange-energy approximation with correct asymptotic behaviour. *J. Phys. Rev. A* **1988**, *38*, 3098−3100.
82. Perdew, J.P. Density−functional approximation for the correlation energy of the inhomogeneous electron gas. *Phys. Rev. B* **1986**, *33*, 8822−8824.
83. Klamt, A.; Jones, V. Treatment of the outlying charge in continuum solvation models. *J. Chem. Phys*. **1996**, *105*, 9972.
84. Klamt, A.; Jonas, V.; Burger, T.; Lohrenz, J. C. Refinement and Parametrization of COSMO-RS. *J. Phys. Chem. A* **1998**, *102*, 5074–5085.
85. B. Delley, The conductor-like screening model for polymers and surfaces. *Mol. Simul*. **2006**, *32*, 117–123.

86. Morokuma, K. Molecular Orbital Studies of Hydrogen Bonds. III. C=O···H–O Hydrogen Bond in $H_2CO···H_2O$ and $H_2CO···2H_2O$. *J. Chem. Phys*., **1971**, *55*, 1236.
87. Kitaura, K.; Morokuma, K. A new energy decomposition scheme for molecular interactions within the Hartree-Fock approximation. *Int. J. Quant. Chem*., **1976**, *10*, 325–340.
88. Ziegler, T.; Rauk, A. On the calculation of multiplet energies by the Hartree-Fock-Slater method. *Theor. Chim. Acta,* **1977***, 43,* 261–271.